Input connectivity reveals additional heterogeneity of dopaminergic reinforcement in *Drosophila*

Nils Otto[1], Markus W. Pleijzier[2], Isabel C. Morgan[1], Amelia J. Edmondson-Stait[2], Konrad J. Heinz[2], Ildiko Stark[2], Georgia Dempsey[2], Masayoshi Ito[3], Ishaan Kapoor[1], Joseph Hsu[3], Philipp M. Schlegel[2,4], Alexander S. Bates[2,4], Marta Costa[2], Kei Ito[5], Davi D. Bock[3,6], Gerald M Rubin[3], Gregory S. X. E. Jefferis[2,4], Scott Waddell[1*]

[1] Centre for Neural Circuits and Behaviour, The University of Oxford, Tinsley Building, Mansfield Road, Oxford, OX1 3SR, UK
[2] Drosophila Connectomics, Department of Zoology, University of Cambridge, CB2 3EJ, UK.
[3] Janelia Research Campus, Howard Hughes Medical Institute, Ashburn, VA 20147, USA
[4] Division of Neurobiology, MRC Laboratory of Molecular Biology, Cambridge CB2 0QH, UK
[5] Institute for Zoology, University of Cologne, Zülpicher Straße 47b, 50674 Cologne, Germany
[6] Current address: Department of Neurological Sciences, University of Vermont Medical Center, VT 05405, USA

*Correspondence and Lead Contact: scott.waddell@cncb.ox.ac.uk
Twitter: @_Nils_Otto_, @mwpleijzier, @scottishwaddell, @gsxej, @dddavi

Highlights

- Nanoscale anatomy reveals additional subclasses of rewarding dopaminergic neurons.
- Connectomics reveals extensive input specificity onto subclasses of dopaminergic neurons.
- Presynaptic arbor morphology suggests a subcompartment resolution for dopaminergic function.
- Aversive memory extinction and sugar learning are served by different subclasses.

Summary

Different types of *Drosophila* dopaminergic neurons (DANs) reinforce memories of unique valence and provide state-dependent motivational control [1]. Prior studies suggest that the compartment architecture of the mushroom body (MB) is the relevant resolution for distinct DAN functions [2, 3]. Here we used a recent electron microscope volume of the fly brain [4] to reconstruct the fine anatomy of individual DANs within three MB compartments. We find the 20 DANs of the γ5 compartment, at least some of which provide reward teaching signals, can be clustered into 5 anatomical subtypes that innervate different regions within γ5. Reconstructing 821 upstream neurons reveals input selectivity, supporting the functional relevance of DAN sub-classification. Only one PAM-γ5 DAN subtype (γ5fb) receives direct recurrent input from γ5β´2a mushroom body output neurons (MBONs) and behavioral experiments distinguish a role for these DANs in memory revaluation from those reinforcing sugar memory. Other DAN subtypes receive major, and potentially reinforcing, inputs from putative gustatory interneurons or lateral horn neurons, which can also relay indirect feedback from the MB. We similarly reconstructed the single aversively reinforcing PPL1-γ1pedc DAN. The γ1pedc DAN inputs are mostly different to those of γ5 DANs and are clustered onto distinct branches of its dendritic tree, presumably separating its established roles in aversive reinforcement and appetitive motivation [5, 6]. Additional tracing identified neurons that provide broad input to γ5, β´2a and γ1pedc DANs suggesting that distributed DAN populations can be coordinately regulated. These connectomic and behavioral analyses therefore reveal additional complexity of dopaminergic reinforcement circuits between and within MB compartments.

Keywords

Learning and Memory, Extinction, Connectomics, Drosophila, Dopamine, Mushroom Body

Results and Discussion

In adult *Drosophila*, anatomically discrete classes of dopaminergic neurons (DANs) innervate adjacent compartments of the mushroom body (MB) lobes [2]. In some cases, it is clear that different combinations of DANs serve discrete roles. However, there are instances where multiple functions have been assigned to DANs that innervate the same compartment. For example, DANs innervating the γ5 compartment reinforce short-term courtship memories, appetitive memories with sugar and they also signal the absence of expected shock, to extinguish aversive memory [7-11]. Similarly, DANs innervating the β´2a compartment have been assigned roles, such as controlling thirst state-dependent water seeking and water memory expression, sugar reinforcement and hunger-dependent modulation of carbon dioxide avoidance [9, 10, 12-14]. Moreover, the individual PPL1-γ1pedc DANs, which innervate the γ1 compartment in both hemispheres are required to reinforce aversive memories with electric shock, high heat and bitter taste, and also provide hunger state-dependent motivational control of sugar memory expression [5, 6, 15, 16]. For an individual DAN to multi-task it must function in different modes. However, where a compartment is innervated by multiple DANs it is unclear whether different neurons in the population perform discrete functions, and/or whether the group functions together in different modes. Here we used connectomics to investigate the organization of synaptic input to DANs innervating the γ5, γ1 and β´2a compartments to better understand how valence-specific reinforcement is generated.

Determining the nanoscale structure of reinforcing dopaminergic neurons

We used a recent EM dataset of a Full Adult Fly Brain (FAFB) [4] to identify, manually trace and reconstruct the nanoscale anatomy of all 20 DANs in the Protocerebral Anterior Medial (PAM) cluster whose presynaptic arbors innervate the γ5 compartment (the PAM-γ5 DANs [2]) in the fly's right brain hemisphere (we also reconstructed 9 PAM-γ5 DANs in the left MB). We then traced 4 of the 10 right hemisphere PAM-β´2a DANs and the 2 Protocerebral Posterior Lateral (PPL)1-γ1pedc DANs that innervate the γ1 compartments of each MB (Figure 1A and S1A-C. Metrics of quality control are detailed in Methods).

We noticed when reconstructing PAM-γ5 DANs that their dendrites appeared to occupy different areas of the superior medial protocerebrum (SMP) [17], that their somas were connected via 2 main neurite tracts, and that each γ5 DAN had a contralateral projection that crossed the midline of the brain in either an upper, middle, or lower commissure (Figures 1A, C-G and S1A, and S1D-S1G). We

therefore used unbiased anatomical clustering to explore a potential suborganisation of PAM-γ5 DANs (Figure 1B). This analysis grouped PAM-γ5 DANs into 5 discrete clusters comprised of 1-7 neurons (Figures 1C-1G). Although we did not trace all the fine axonal branches of the PAM-γ5 DANs it was evident that their major presynaptic arbors occupy different areas of the γ5 compartment. We therefore named the PAM-γ5 DAN subclusters according to their defining morphological feature.

The 4 traced PAM-β´2a DANs could also be clustered into 3 subgroups with commissure crossed, overall morphology and the region of the compartment that is innervated again being the primary distinguishing features (Figures 1B, 1H-1J and S1B, and S1D-S1G). Our tracing also identified a 'non-canonical' PAM-β´2a DAN, which mostly innervates β´2a but also extends presynaptic processes into the γ5 compartment (Figure 1J). The dendrites of PAM-β´2a DANs were largely intermingled with those of the PAM-γ5 DANs (Figures 1C-J), consistent with their roles in reinforcing appetitive memories.

Reconstructing the individual right hand PPL1-γ1pedc DAN revealed that its dendrites occupy very different locations to that of the PAM-γ5 and PAM-β´2a DANs (Figure 1K). This suggests that PPL1-γ1pedc receives mostly different input, consistent with it signalling aversive rather than appetitive valence. The three-dimensional structure of the PPL1-γ1pedc DAN dendrite shows four major arbors that extend into discrete locations in the brain (Figures 1L and M, and S1H). Post-synapses also clustered in each of these locations suggesting that PPL1-γ1pedc DANs could receive branch-specific information. This may represent a solution for how a single PPL1-γ1pedc DAN can isolate and prioritize its discrete roles in reinforcement and state-dependent control [5, 6].

Mapping neuronal inputs onto dopaminergic neurons

We next traced 821 neurons providing input to post-synapses identified in the dendritic arbors of the PAM-γ5, PAM-β´2a and PPL1-γ1pedc DANs (Figure 2A). Since connectivity is dense and manual tracing is very labor-intensive we aimed to trace at least 50% of the inputs to all reconstructed DANs. We prioritized upstream tracing so we retrieved a comparable coverage of the inputs to each of the major morphological DAN subclasses. Criteria for sampling and metrics of quality control are again detailed in the Methods.

Reassuringly, the input selectivity of the PAM-γ5, PAM-β´2a and PPL1-γ1pedc DANs largely reflected the relative overlap of their dendritic fields. All the DANs were found to receive unique inputs (Figure 2B-C, and S2A-D). However, a greater share of the 553 identified inputs to PAM-γ5 DANs (181) also provided inputs to PAM-β´2a DANs than to the PPL1-γ1pedc DAN (88). Likewise, more of the 485 PAM-β´2a DANs inputs made synapses with PAM-γ5 DANs (181) than with the PPL1-γ1pedc DAN (67). In contrast more of the 275 traced PPL1-γ1pedc DAN inputs were unique (168) than also contacted PAM-γ5 DANs (84) or PAM-β´2a DANs (67). Lastly, 8% (44) of the traced input neurons made synapses onto all three classes of traced DANs. These common input neurons suggest that the valence specific arms of the DAN system may also be coordinately regulated under certain contexts. It is however also possible that the different DANs respond in unique ways to the same input neurotransmitters.

Our sampling suggests that despite there being 20 PAM-γ5 DANs and one PPL1-γ1ped DAN, there are only approximately twice as many inputs to all PAM-γ5 DANs than to the PPL1-γ1pedc DAN (Figure 2B). However, assuming that synapse number correlates with input strength, we found that the different DAN classes had a markedly different weighting of inputs (Figure 2D and S2E). Whereas the PPL1-γ1pedc DAN receives weakly connected inputs, each input to the PAM-γ5 DANs or PAM-β´2a DANs is more strongly connected and contributes a larger proportion of the individual neuron's postsynaptic budget. Plotting a connectivity matrix for the most completely traced DANs reveals that certain groups of inputs preferentially synapse onto different PAM-γ5 and PAM-β´2a DANs, demonstrating that all individual PAM-γ5 and PAM-β´2a DANs have an element of input specificity (Figure 2E). Nevertheless, a matrix comparing input structure between DANs reveals significant similarities in input between particular groups of PAM-γ5 and PAM-β´2a DANs (Figure 2F, and S2F-H). It is notable that DAN clustering based on dendritic connectivity correlated well with the prior clustering using full neuron morphology (Figure 1B, 2H, and S2F-I). This correlation suggests that information conveyed in input specificity is likely to be maintained in the activity of different classes of DANs.

We next performed a clustering analysis of the input neurons based on their morphology. In a 3-step approach (Figure S2J) we focused first on soma location and primary neurite layout. This revealed 20 major neuronal clusters (Figure 2I), which could be further decomposed through 2 additional steps into 285 clusters distinguished by the detailed anatomy of smaller neurites (Figure S2J). We focused

our initial analyses on four classes of input neurons, for which we could postulate a functional role; MBONs, Lateral horn associated neurons that include Lateral Horn Output Neurons (LHONs), SEZONs – potential gustatory projection neurons which ascend from the subesophageal zone (SEZ), and OTHERs – a variety of single neurons conveying information from other interesting brain areas (Figure 2I-J).

Annotating the DAN clustering with the identity of input neurons revealed that the γ5β´2a MBONs specifically provide feedback (fb) input from the MB to our previously defined PAM-γ5dd cluster (green segments in Figure 2K). We therefore renamed the PAM-γ5dd neurons as PAM-γ5fb. Other MBONs (red) also provide selective input to different DANs. In contrast, as a group the SEZONs (blue) and LHONs (yellow) provide input to the PPL1-γ1pedc DAN and all PAM-γ5 and PAM-β´2a DANs, although the relative proportions vary considerably.

Towards assigning functional relevance to the identified input pathways, we first used NBLAST [18] to screen traced neuronal skeletons against a collection of confocal volumes of GAL4 and split-GAL4 lines for those that potentially drive expression in the relevant neurons [19] [20] [21] (Figure 2L). This analysis identified >50 driver fly lines with putative expression in the major SEZONs, LHONs, MBONs and OTHERs groups of DAN inputs.

Functional analyses of input pathways to DANs

Pairing odor exposure with optogenetic activation of PPL1-γ1pedc or PAM-γ5, PAM-β´2a DANs can produce either aversive or appetitive odor memories, respectively [22]. We therefore assumed that neurons providing significant input to reinforcing neurons should be able to generate similar phenotypes if artificially engaged, instead of the relevant DANs. We therefore combined all the GAL4 driver lines with the red-light activated UAS-CsChrimson [23] optogenetic trigger and screened them for their potential to reinforce olfactory memories by pairing their artificial activation with odor exposure (Figure 3A and S3A). We obtained a broad range of phenotypes. Whereas some GAL4 lines produced robust appetitive odor memories, others produced aversive memories, and some had apparently no consequence. We also correlated the identity of neurons labelled in each GAL4 line that produced significant memory performance (generally above or below a PI of +/-0.1) with their respective DAN connectivity (Figure 3B). These correlations revealed good concordance with the valence of the memories formed by MBONs and SEZONs (see below and Figures 3H and 3I for follow-up). We found 3 different LHON types that connect to γ5 DANs

and not PPL1-γ1pedc DANs and form appetitive memories; LHON01, LHON02 and LHON-AD1b2 (Figure 3A; [24, 25]), and the OTHER line15 formed aversive memory and preferentially synapses with PPL1-γ1pedc (Figure 3A and B). For all input to DAN connectivity we predict that even incompletely sampled DANs would, if traced further, not connect to new neurons but only increase the strength to known partners (Figure S3B).

MBON-DAN connectivity

Two MBONs have previously been described that have a dendrite in the γ5 compartment, MBON- γ5β´2a and MBON-γ4γ5 [3] [11]. In the stimulus replacement screen these MBONs appeared to convey opposite valence. Whereas MBON-γ5β´2a activation formed appetitive memory, MBON-γ4γ5 activation reinforced aversive memory (Figure 3A; and confirmatory 30 min memory experiment in Figure S3C). Connectivity supported these behavioral results. MBON-γ4γ5 has many (32) synapses onto PPL1-γ1pedc but not PAM-γ5 or PAM-β´2a DANs, while MBON-γ5β´2a synapses onto PAM-γ5fb and a PAM-β´2a DAN but not PPL1-γ1pedc DANs (Figure 3B-C and Figure S3D).

Our tracing of DAN inputs also identified selective connectivity with a few additional MBONs (Figure 3C). MBON-α´2 was found to synapse onto PAM-β´2a and PAM-γ5ba and -γ5uc DANs, MBON-β´2mp with PAM-γ5lc, MBON-γ2α´1 with PAM-β´2a, and MBON-γ3β´1 with PAM-β´2a and PAM-γ5uc. With a few exceptions, this relatively sparse connectivity of these MBONs to our traced DANs was largely maintained when we included other traced neurons as potential interneurons between them (Figure 3D). Most notably, the apparent bias of connection of MBON-γ4γ5 to PPL1-γ1pedc and the selectivity of MBON-γ3β´1 remained and new selective clusters to our PAM-γ5fb, uc, and PAM-β´2a groups became apparent. No indirect connections were detected between MBON-γ4γ5 and PPL1-γ1pedc. Moreover, only one additional β´2a DAN was seen to be downstream of MBON-γ4γ5 when putative indirect connectivity was included. In contrast, although we found MBON-γ5β´2a to be directly connected to only the PAM-γ5fb DANs it is indirectly connected to most of our other traced DANs, and all of the inputs to the unique PAM-γ5da neuron (Figure 1G) come from neurons downstream of MBON-γ5β´2 (Figure 1G). Axo-axonic synapses are a common feature of the DAN input network. MBONs frequently make reciprocal synapses on the axons of SEZONs and LHONs. The different classes of

DAN input neurons are also highly interconnected within cluster by axo-axonic synapses.

SEZON-DAN connectivity

Synthetic activation of the SEZON lines also produced different learning phenotypes. Activation of SEZON01 neurons formed aversive memory and these connect to PPL1-γ1pedc and some PAM-γ5, but not to γ5 DANs reinforcing sugar memory (see below). Stimulating the SEZON03 neurons formed appetitive memory and these SEZONs have synapses onto PAM-γ5 but not PPL1-γ1pedc. SEZON02 neuron activation did not implant significant memory of either valence and appears to connect weakly to all three classes of traced DANs (Figure 3A and B, and S3I)).

Despite their specificity, we expect some of our identified GAL4 drivers to express in our traced neurons of interest, and additional similar neurons in a bundle. For example, a SEZON line could label a collection of ascending neurons that represent both tasteful and distasteful gustatory stimuli [26]. Labelling such a mixed population with contradictory value, could explain the inability of SEZON2 to reinforce a memory with clear valence. We therefore used the dominant temperature sensitive UAS-*Shibire*^{ts1} transgene [27] to block neurotransmission from the SEZ neurons during training with sugar or bitter taste reinforcement (Figures 3E-F and S3E-I). We included R58E02-GAL4 as a positive control for sugar memory, which expresses in the majority of PAM DANs [28] and MB320C-GAL4 for bitter learning, as it expresses in PPL1-γ1pedc [29]. Blocking R58E02 or SEZON03 neurons during training abolished 30 min memory reinforced with sugar but blocking SEZON01 and SEZON02 neurons had no impact. In contrast, blocking MB320C, SEZON01 or SEZON02, but not SEZON03 neurons impaired 30 min memory after bitter learning. These data support a role for SEZONs in relaying positive and negative gustatory valence to subclasses of DANs.

Analysis of the location of identified inputs to the PPL1-γ1pedc DAN confirmed that it receives branch-specific information (Figures 3G and S3J-H). Whereas all aversively reinforcing input from SEZONs in SEZ1 connect to the arbor in SMP, the line 15 OTHER neurons, which can also produce aversive reinforcement, connect to the PPL1-γ1pedc DAN arbor in the ventral and dorsal crepine (CRE) [17]. MBON input in general and the strong MBON-γ4γ5 inputs are also mostly found on the CRE_v and CRE_d branches of PPL1-γ1pedc. Since these branches are the closest to the primary axon, input from other MB compartments may be particularly salient to PPL1-γ1pedc

(Figure S3J). Interestingly, the strongest input from MBON-γ5β´2a to the PAM-γ5fb DANs are similarly placed on the DAN dendrite (Figure S4A).

Functional subdivision of PAM-γ5 DANs

Based on prior findings, we hypothesized that PAM-γ5fb DANs which receive recurrent feedback from MBON-γ5β´2a would be required for memory revaluation [11] and other PAM-γ5 DANs receiving input from SEZONs labelled by SEZON03 would be required to reinforce sugar memory [9]. Testing this model required locating GAL4 drivers that label subsets of γ5 DANs that at least partially correspond to functionally relevant subgroups. We therefore used the specificity of commissure crossing to select GAL4 drivers, some of which have previously been reported to express in subsets of PAM-γ5 DANs [9]. We reasoned that drivers labelling the lower commissure might express in γ5fb-DANs (Figure 1E) and others labelling the upper commissure could include γ5-DANs connected to the appropriate sugar-selective SEZONs. We identified VT06202-GAL4 (Figure 4A), which expresses in γ5-DANs in all 3 commissures, MB315C- (Figure 4B) and 0804-GAL4s (Figure 4C), which express in 8 and 3-5 γ5 DANs respectively in the lower commissure, and 0104-GAL4 (Figure 4D), which only expresses in upper commissure γ5 DANs [2, 9, 21, 30]. We also used genetic intersection with GAL80 to restrict 0104-GAL4 expression to γ5b and β´2m (Figure 4E, [9, 12]).

We next tested whether blocking the neurons labelled in these GAL4s with UAS-*Shi*^{ts1} disrupted aversive memory extinction and/or sugar learning (Figures 4G and H). We again used the broad PAM DAN expressing R58E02-GAL4 as a control. To assay extinction of aversive memory (Figure 4F, controls in Figure S4D), flies were differentially conditioned by pairing one of two odors with electric shock [31]. Then 30 min after training they received two un-reinforced exposures of the previously shock paired odor (CS+) or the other odor (CS-) at 15 min interval [11]. They were then left undisturbed for 15 min before being tested for olfactory preference memory. As previously established, only re-exposure to the CS+ odor diminished memory performance, demonstrating odor-specific memory extinction. We blocked subsets of DANs specifically during odor re-exposure by training flies at permissive 25˚C, transferring them to restrictive 32˚C immediately after training, then returning them to 25˚C after the second odor re-exposure. Blocking R58E02, VT006202 and 0804 neurons abolished memory extinction, whereas memory was still extinguished in flies with blocked MB315C or 0104 neurons (+ and - GAL80). No extinction was observed in any line when flies were re-exposed to the CS- odor after training. These data

support a role for the 0804-GAL4 group of lower commissure PAM-γ5fb DANs in memory extinction (Figure 3F).

In contrast, when these neurons were selectively blocked only during sugar (sucrose) conditioning [32] (Figure 4G, controls in Figures S4E and F), 30 min memory was impaired in R58E02, VT00602 and 0104 (+ and – GAL80) flies expressing UAS-*Shi*^{ts1}, but was unaffected in UAS-*Shi*^{ts1} expressing MB315C and 0804 flies (Figure 3G). These data demonstrate that memory extinction and sucrose reinforcement are dissociable in the γ5 DANs and support the selective role for PAM-γ5fb DANs in memory extinction and SEZON connected PAM-γ5 DANs in sucrose reinforcement (Figure 4H). We therefore propose that the other morphological classes of PAM-γ5 DANs may also serve different functions.

The morphologically distinct classes of γ5 DANs innervate different regions of the γ5 compartment where they could depress or potentiate different parts of the KC-MBON network (Figure 1C-G and S4B) [29, 33, 34]. We do not currently understand the full relevance of the sub-compartment architecture. However, since the γ-lobe dorsal (γd) KCs carry visual information and the main γ KCs are olfactory [35], connections of these two streams of KCs to γ5 MBONs could be independently modified by PAM-γ5da (Figure 1G) and PAM-γ5dd/fb DANs (Figure 1E), whose processes are confined to the respective subregions of the γ5 compartment. DAN stratification may therefore be important for maintaining modality specificity of olfactory memory revaluation [11]. It is interesting to note that larvae only have one DAN per MB compartment [36] and that multiple DANs per compartment is an adult-specific specialization [2]. We expect this expansion reflects the additional behavioral demands of the adult fly and our work here suggests the larger number of DANs in each compartment likely provides additional functional capacity to the compact anatomy of the adult MB.

References

1. Cognigni, P., Felsenberg, J., and Waddell, S. (2017). Do the right thing: neural network mechanisms of memory formation, expression and update in Drosophila. Curr Opin Neurobiol. *49*, 51-58.
2. Aso, Y., Hattori, D., Yu, Y., Johnston, R.M., Iyer, N.A., Ngo, T.T., Dionne, H., Abbott, L.F., Axel, R., Tanimoto, H. et al. (2014). The neuronal architecture of the mushroom body provides a logic for associative learning. Elife. *3*, e04577.
3. Aso, Y., Sitaraman, D., Ichinose, T., Kaun, K.R., Vogt, K., Belliart-Guerin, G., Placais, P.Y., Robie, A.A., Yamagata, N., Schnaitmann, C. et al. (2014). Mushroom body output neurons encode valence and guide memory-based action selection in Drosophila. Elife. *3*, e04580.
4. Zheng, Z., Lauritzen, J.S., Perlman, E., Robinson, C.G., Nichols, M., Milkie, D., Torrens, O., Price, J., Fisher, C.B., Sharifi, N. et al. (2018). A Complete Electron Microscopy Volume of the Brain of Adult Drosophila melanogaster. Cell. *174*, 730-743.e22.
5. Krashes, M.J., DasGupta, S., Vreede, A., White, B., Armstrong, J.D., and Waddell, S. (2009). A neural circuit mechanism integrating motivational state with memory expression in Drosophila. Cell. *139*, 416-427.
6. Aso, Y., Siwanowicz, I., Bracker, L., Ito, K., Kitamoto, T., and Tanimoto, H. (2010). Specific dopaminergic neurons for the formation of labile aversive memory. Curr Biol. *20*, 1445-1451.
7. Keleman, K., Vrontou, E., Kruttner, S., Yu, J.Y., Kurtovic-Kozaric, A., and Dickson, B.J. (2012). Dopamine neurons modulate pheromone responses in Drosophila courtship learning. Nature. *489*, 145-149.
8. Zhao, X., Lenek, D., Dag, U., Dickson, B.J., and Keleman, K. (2018). Persistent activity in a recurrent circuit underlies courtship memory in Drosophila. Elife. *7*,
9. Huetteroth, W., Perisse, E., Lin, S., Klappenbach, M., Burke, C., and Waddell, S. (2015). Sweet taste and nutrient value subdivide rewarding dopaminergic neurons in Drosophila. Curr Biol. *25*, 751-758.
10. Yamagata, N., Ichinose, T., Aso, Y., Placais, P.Y., Friedrich, A.B., Sima, R.J., Preat, T., Rubin, G.M., and Tanimoto, H. (2015). Distinct dopamine neurons mediate reward signals for short- and long-term memories. Proc Natl Acad Sci U S A. *112*, 578-583.
11. Felsenberg, J., Jacob, P.F., Walker, T., Barnstedt, O., Edmondson-Stait, A.J., Pleijzier, M.W., Otto, N., Schlegel, P., Sharifi, N., Perisse, E. et al. (2018). Integration of Parallel Opposing Memories Underlies Memory Extinction. Cell. *175*, 709-722.e15.

12. Lin, S., Owald, D., Chandra, V., Talbot, C., Huetteroth, W., and Waddell, S. (2014). Neural correlates of water reward in thirsty Drosophila. Nat Neurosci. *17*, 1536-1542.
13. Senapati, B., Tsao, C.H., Juan, Y.A., Chiu, T.H., Wu, C.L., Waddell, S., and Lin, S. (2019). A neural mechanism for deprivation state-specific expression of relevant memories in Drosophila. Nat Neurosci. *22*, 2029-2039.
14. Lewis, L.P., Siju, K.P., Aso, Y., Friedrich, A.B., Bulteel, A.J., Rubin, G.M., and Grunwald Kadow, I.C. (2015). A Higher Brain Circuit for Immediate Integration of Conflicting Sensory Information in Drosophila. Curr Biol. *25*, 2203-2214.
15. Galili, D.S., Dylla, K.V., Ludke, A., Friedrich, A.B., Yamagata, N., Wong, J.Y., Ho, C.H., Szyszka, P., and Tanimoto, H. (2014). Converging circuits mediate temperature and shock aversive olfactory conditioning in Drosophila. Curr Biol. *24*, 1712-1722.
16. Das, G., Klappenbach, M., Vrontou, E., Perisse, E., Clark, C.M., Burke, C.J., and Waddell, S. (2014). Drosophila learn opposing components of a compound food stimulus. Curr Biol. *24*, 1723-1730.
17. Ito, K., Shinomiya, K., Ito, M., Armstrong, J.D., Boyan, G., Hartenstein, V., Harzsch, S., Heisenberg, M., Homberg, U., Jenett, A. et al. (2014). A systematic nomenclature for the insect brain. Neuron. *81*, 755-765.
18. Costa, M., Manton, J.D., Ostrovsky, A.D., Prohaska, S., and Jefferis, G.S. (2016). NBLAST: Rapid, Sensitive Comparison of Neuronal Structure and Construction of Neuron Family Databases. Neuron. *91*, 293-311.
19. Gohl, D.M., Silies, M.A., Gao, X.J., Bhalerao, S., Luongo, F.J., Lin, C.C., Potter, C.J., and Clandinin, T.R. (2011). A versatile in vivo system for directed dissection of gene expression patterns. Nat Methods. *8*, 231-237.
20. Jenett, A., Rubin, G.M., Ngo, T.T., Shepherd, D., Murphy, C., Dionne, H., Pfeiffer, B.D., Cavallaro, A., Hall, D., Jeter, J. et al. (2012). A GAL4-driver line resource for Drosophila neurobiology. Cell Rep. *2*, 991-1001.
21. Tirian, L., and Dickson, B.J. (2017). The VT GAL4, LexA, and split-GAL4 driver line collections for targeted expression in the Drosophila nervous system. bioRxiv. 198648.
22. Aso, Y., and Rubin, G.M. (2016). Dopaminergic neurons write and update memories with cell-type-specific rules. Elife. *5*,
23. Klapoetke, N.C., Murata, Y., Kim, S.S., Pulver, S.R., Birdsey-Benson, A., Cho, Y.K., Morimoto, T.K., Chuong, A.S., Carpenter, E.J., Tian, Z. et al. (2014). Independent optical excitation of distinct neural populations. Nat Methods. *11*, 338-346.

24. Dolan, M.J., Belliart-Guerin, G., Bates, A.S., Frechter, S., Lampin-Saint-Amaux, A., Aso, Y., Roberts, R.J.V., Schlegel, P., Wong, A., Hammad, A. et al. (2018). Communication from Learned to Innate Olfactory Processing Centers Is Required for Memory Retrieval in Drosophila. Neuron. *100*, 651-668.e8.
25. Dolan, M.J., Frechter, S., Bates, A.S., Dan, C., Huoviala, P., Roberts, R.J., Schlegel, P., Dhawan, S., Tabano, R., Dionne, H. et al. (2019). Neurogenetic dissection of the Drosophila lateral horn reveals major outputs, diverse behavioural functions, and interactions with the mushroom body. Elife. *8*,
26. Scott, K. (2005). Taste recognition: food for thought. Neuron. *48*, 455-464.
27. Kitamoto, T. (2001). Conditional modification of behavior in Drosophila by targeted expression of a temperature-sensitive shibire allele in defined neurons. J Neurobiol. *47*, 81-92.
28. Liu, C., Placais, P.Y., Yamagata, N., Pfeiffer, B.D., Aso, Y., Friedrich, A.B., Siwanowicz, I., Rubin, G.M., Preat, T., and Tanimoto, H. (2012). A subset of dopamine neurons signals reward for odour memory in Drosophila. Nature. *488*, 512-516.
29. Hige, T., Aso, Y., Modi, M.N., Rubin, G.M., and Turner, G.C. (2015). Heterosynaptic Plasticity Underlies Aversive Olfactory Learning in Drosophila. Neuron. *88*, 985-998.
30. Burke, C.J., Huetteroth, W., Owald, D., Perisse, E., Krashes, M.J., Das, G., Gohl, D., Silies, M., Certel, S., and Waddell, S. (2012). Layered reward signalling through octopamine and dopamine in Drosophila. Nature. *492*, 433-437.
31. Tully, T., and Quinn, W.G. (1985). Classical conditioning and retention in normal and mutant Drosophila melanogaster. J Comp Physiol [A]. *157*, 263-277.
32. Krashes, M.J., and Waddell, S. (2008). Rapid consolidation to a radish and protein synthesis-dependent long-term memory after single-session appetitive olfactory conditioning in Drosophila. J Neurosci. *28*, 3103-3113.
33. R, C., I, M., and V, R. (2015). Coordinated and compartmentalized neuromodulation shapes sensory processing in Drosophila. Cell.
34. Handler, A., Graham, T.G.W., Cohn, R., Morantte, I., Siliciano, A.F., Zeng, J., Li, Y., and Ruta, V. (2019). Distinct Dopamine Receptor Pathways Underlie the Temporal Sensitivity of Associative Learning. Cell. *178*, 60-75.e19.
35. Vogt, K., Aso, Y., Hige, T., Knapek, S., Ichinose, T., Friedrich, A.B., Turner, G.C., Rubin, G.M., and Tanimoto, H. (2016). Direct neural pathways convey distinct visual information to Drosophila mushroom bodies. Elife. *5*,

36. Eichler, K., Li, F., Litwin-Kumar, A., Park, Y., Andrade, I., Schneider-Mizell, C.M., Saumweber, T., Huser, A., Eschbach, C., Gerber, B. et al. (2017). The complete connectome of a learning and memory centre in an insect brain. Nature. *548*, 175-182.

Acknowledgements

We are grateful to other members of the Waddell and Jefferis groups for discussion and input throughout this project. This work was largely funded by S.W., G.S.X.E.J., D.B. and G.M.R. through a Wellcome Collaborative Award (203261/Z/16/Z). S.W. is also supported by a Wellcome Principal Research Fellowship (200846/Z/16/Z), the Gatsby Charitable Foundation (GAT3237) and an ERC Advanced Grant (789274).

Figure Legends

Figure 1. Nanoscale morphology of PAM-γ5, PAM-β´2a and PPL1-γ1pedc DANs reveals new anatomical classes and features.

(A) Representation of all DANs reconstructed in this study. 20 PAM-γ5 DANs on the fly's right and 9 on the left, 10 PAM-β´2a DANs on the right, and both left and right PPL1-γ1pedc DANs are shown. The MB and overall brain are outlined. (B) Dendrogram showing average linkage clustering of PAM DANs by Euclidean distance between their NBLAST. 5 PAM-γ5 DAN and 3 β´2a DAN clusters are evident.. (C) Projection view of the 6 DANs of the PAM-γ5lc cluster (blue). In panels C-K, the morphology of the other traced PAM-γ5, PAM-β´2a DANs are shown in overlap (grey). (D) Projection view of the 5 DANs of the PAM-γ5uc cluster (green). (E) Projection view of the 3 DANs of the PAM-γ5dd cluster (scarlet). We show in Figure 2J that only these neurons receive feedback from MBON-γ5β´2a and from thereon rename these DANs PAM-γ5fb. (F) Projection view of the 2 DANs of the PAM-γ5ba cluster (lilac). These DANs occupy the middle commissure. (G) Projection view of the single PAM-γ5da DAN (purple). (H) Projection view of a PAM-β´2amc DAN (lime) which also occupies the middle commissure. (I) Projection view of two PAM-β´2lc DANs (turquoise). (J) Projection view of a non-canonical PAM-β´2nc DAN (navy). (K) Projection view of a PPL1-γ1pedc DAN (maroon). (L) Clustering of PPL1-γ1pedc DAN post-synapses in 3D space generates 4 distinct groups localized in the SIP (superior intermediate protocerebrum), SMP and CREd and CREv. The optimum number of clusters was determined by the elbow method, see Figure S1H. (M) Correlation of postsynapse clusters with PPL1-γ1pedc dendritic branches shown on a 2-dimensional neato dendrogram. Inset: 3D projection illustrating well separated dendritic branches in colors corresponding to the postsynapse clusters.

Figure 2. Input specificity to dopaminergic neurons matches anatomical subtypes.

(A) Representation of all 821 input neurons to PAM-γ5, PAM-β´2a, and PPL1-γ1pedc DANs identified in this study. Cell bodies are shown as black spheres and processes in grey. DANs and the MB outline are shown for reference (compare to Figure 1A). (B) Venn diagram of unique and common inputs to the analyzed DANs. PPL1-γ1pedc receives largely different input to that of PAM-γ5 and PAM-β´2a DANs. PAM-γ5 and PAM-β´2a DANs have many common inputs and some of these are also shared by PPL1-γ1pedc. (C) Venn diagrams showing percentage of postsynaptic budget occupied by shared and unique input neurons to PAM-γ5, PAM-β´2a, and PPL1-γ1pedc DANs. Almost 15% of both PPL1-γ1pedc and PAM-β´2a are common to all groups. For PAM-γ5 DANs this number falls to 8%. (D) Bar chart showing DANs have many inputs with very low edge weight and each representing a small fraction of their overall postsynaptic budget. Inputs contributing more of the postsynaptic budget (to the right of the graph) are more abundant for PAM-γ5 and PAM-β´2a DANs, the PPL1-γ1pedc distribution is strongly left shifted. (E) DANs can be clustered by input connectivity (dendrogram to the right of panel F). Heatmap shows that every DAN has a group of unique input neurons - unique blocks in each row. Clustering of DANs mostly depends on lesser number of shared inputs compressed to the left edge of the heatmap. (F) A DAN similarity matrix where DANs are grouped by the similarity of their input connectivity has clear structure, that is significantly more organized than random connectivity (comparison to null-model, Figure S2F-G: $p < 0.0001$, Mantel test,). (G) Representation of traced input neurons labelled using the unique and common input anatomy determined in panel 2B (also see Figure S2A-D for separate classes). (H) A tanglegram comparing DAN clustering by morphology (Figure 1B) and clustering by input connectivity (dendrogram in F). Neither grouping is significantly independent of the other (Pearsons Correlation: $r=0.604$, Mantel Test: $p<e\text{-}7$; also $p_w<e\text{-}7$ within only γ5 or β´2a group (for Mantel Test see: Figure S2I). (I) DAN input neurons clustered by morphology using a 3-step process (Figure S2J). Dendrogram below shows single neurons allocated to 20 major clusters based on soma position and primary neurite tract. Their approximate neuropil of origin is indicated. AL, antennal lobe multiglomerular olfactory projection neurons that only connect to PPL1-γ1pedc. Many neurons originate from less explored neuropil (misc). (J) Fine clusters of exemplary neurons for the MBON, LHON, SEZON and OTHER classes of DAN inputs. (K) Barplot showing respective number of MBON, LHON, SEZON and OTHER inputs to individual DANs, ordered according to cluster identity (Figure 1). In general, PAM-γ5 DANs receive about 35%

of their inputs from SEZONs, and about 20% from LHONs. Only the 3 PAM-γ5fb DANs receive significant direct input from MBON-γ5β´2a (green segments). PAM-β´2 DANs receive about 15% from SEZONs and about 35% from LHONs. One PAM-β´2a DAN also receives minor direct input from MBON-γ5β´2a. PPL1-γ1pedc DANs receive roughly equal LHON and SEZON input. (L) NBLAST compares CATMAID generated neuronal skeletons from FAFB to neurons labelled in confocal images of GAL4 expression patterns.

Figure 3. Functional analyses of DAN input neurons.

(A) 49 GAL4 driver lines with identified DAN input neurons were used to drive UAS-CsChrimson and screened for memory implantation by pairing neural activation with odor exposure. Flies were starved 18-26 h prior to training and tested for immediate memory performance. n=6-12 per genotype. Lines of interest in this study are labelled (full detail in Figure S3A). (B) Connectivity matrix between DANs ordered according to cluster identity and 10 input neurons whose activation generated a significant phenotype in Figure 3A, corresponding to 11 input clusters (MBON-γ5β´2a and MBON-γ4,γ5, SEZON01-03, LHON01-02, and LHON-AD1b2, and OTHER15-16). Connectivity often corresponds to valence of memory formed. (C) Direct MBON-DAN connectivity matrix. We identified several MBONs to provide input to specific DANs (note: we traced all inputs to 7 PAM-γ5 PAM DANs). (D) Adding other traced DAN input neurons creates the potential for indirect connectivity between some MBONs and specific subsets of DANs. Indirect matrix thresholded above 2 synapses from MBONs to input neurons. (E) Olfactory learning with sucrose reinforcement. Schematic, experimental timeline and temperature shift protocol. Blocking neuron output during training abolished 30 min appetitive memory specifically in SEZON03-GAL4; UAS-*Shi*^{ts1} and R58E02-GAL4; UAS-*Shi*^{ts1} flies ($p<0.0241$ and 0.0089 respectively one-way ANOVA, with Dunnett's post hoc test, n=10). (F) Olfactory learning with bitter (DEET) reinforcement. Schematic, experimental timeline and temperature shift protocol. Blocking neuron output training impaired immediate aversive memory in MB320C-, SEZON01- and SEZON02-GAL4; UAS-*Shi*^{ts1}, but not in SEZON03; UAS-*Shi*^{ts1} flies. ($p<0.0009$, 0.0344, and 0.0170 respectively, one-way ANOVA with Dunnett's post hoc test, n=12). (G) Connectivity matrix to specific branches of the PPL1-γ1pedc dendrite reveals classes of input neurons have branch specificity. (H) Neato dendrogram showing MBON inputs to PPL1-γ1pedc on the CREd and CREv branches and their relative proximity to the proximal axon. MBON-γ4,γ5 provides the most synapses of all MBONs identified to input to PPL1-γ1pedc.

Figure 4. Aversive memory extinction and sugar learning require different subsets of PAM-γ5 DANs.

(A) Brain from a VT006202-GAL4; UAS-GFP fly labels all 20 PAM-γ5 DANs (green). 3 commissures are visible (asterisk). Brain co-stained with nc82 antibody (blue). Scale bar 20µm. (B) MB315C-GAL4; UAS-GFP specifically labels 8 PAM-γ5 DANs per hemisphere that cross the midline in the lower commissure. (C) 0104-GAL4; UAS-GFP labels some PAM-γ5 DANs, previously named 'γ5 broad', that cross the midline in the upper and middle commissures. 0104 also labels some other PAM DANs [9]. (D) 0804-GAL4 labels 5 PAM-γ5 DANs per hemisphere, previously 'γ5 narrow' that occupy the lower commissure. Scale bar 20µm. (E) Table summarizing DAN expression in GAL4 lines used for behavior testing, modified from [9]. R48B04GAL80 refines the 0104-GAL4 expression pattern [12]. (F) Aversive olfactory memory extinction. Schematic, experimental timeline and temperature shift protocol. Blocking neuron output during odor re-exposure impaired memory extinction in R58E02-, VT006202- and 0804-GAL4; UAS-*Shi*^{ts1} but not in MB315C- or 0104 +/- GAL80; UAS-*Shi*^{ts1} flies. Asterisks denote $p<0.035$ (wildtype) and $p<0.0176$ (0104), one-way ANOVA, with Tukey's post hoc test, n=10-12). (G). Olfactory learning with sucrose reinforcement. Schematic, experimental timeline and temperature shift protocol. Blocking neuron output during training impaired 30 min appetitive memory in R58E02-, VT006202- and 0104 +/- GAL80; UAS-*Shi*^{ts1} but not MB315C- or 0804-GAL4; UAS-*Shi*^{ts1} flies. Asterisks denote $p<0.0003$ (R58E02), $p<0.0004$ (0104), $p<0.0018$ (VT006202), and $p<0.0010$ (0104;R48B04GAL80); one-way ANOVA, with Dunnett's post hoc test, n=10). (H) Schematic of input pathways to PAM-γ5 and PAM-β´2a DANs and subcluster innervation of the γ5 compartment.

Supplementary Figure Legends

Figure S1 related to Figure 1

(A-C) Representations of all reviewed DANs in the right hemisphere.
(A) 20 PAM-γ5 DANs on the fly's right. MB is outlined. Asterisk indicates 2 descending tracts correspond to soma tracts and commissures (compare to S1E). (B) 6 PAM-β´2a DNAs in the fly's right hemisphere. (C) The fly's right-hand side PPL1- γ1pedc DAN. Note the elaborate dendrite outside the MB. (D) Dendrogram of morphological clusters. Average linkage clustering of commissure tracts of PAM- γ5 and PAM- β´2a DANs by Euclidean distance between their NBLAST scores. This reveals 3 commissures shown in the dendrogram. (E) Projection view of the 3 commissure groups resulting from clustering in (D), upper commissure: orange, middle commissure: purple, lower commissure: green. Morphologies of the complete neurons are shown in overlap (grey). (F) Average linkage clustering of the descending tracts connecting dendrites and soma tract with the axons in the MB. Using Euclidean distance between NBLAST similarity matrices reveals 2 distinct tracts. Posterior soma tract: purple; and anterior soma tract: green. (G) Projection view of the 2 soma tract groups resulting from clustering in (F), The posterior tract mostly contains neurons from the lower commissure, indicated by the dashed line next to the #. The anterior soma tract mostly contains neurons from the upper commissure. Link indicated by dashed line by the asterisk. (H) Elbow method to determine the optimal number of clusters in hierarchical clustering. The percentage of variance that is accounted for with clustering of x clusters is plotted. An edge, or elbow, can be seen which identifies 4 as the optimum number of clusters. (asterisk).

Figure S2 related to Figure 2

(A-D) Related to Figures 2C and 2G. Representation of neurons unique to (A) PAM-γ5 DANs (green), (B) PPL1-γ1pedc (red). (C) PAM-β´2a DANs (blue). (D) shared input (black). Whole brain outlined in gray for reference. (E) Related to Figure 2D. Absolute (non-normalised) edge weight distribution between input neurons and DANs. The frequency at which an input to a given DAN with a certain number of connections occurs is shown as a function of the number of connections. DANs have many inputs connected with one or few synapses only (on the left). The long tail of the distribution of PPL1-γ1pedc indicates that it has some input partners with high absolute edge weights. (F) Random connectivity null model. CATMAID synaptic connectivity from observed data is represented as a connectivity matrix (left). To create a null model this matrix is randomised

maintaining the row and column sums to conserve the proportion of DAN postsynaptic budget and input presynaptic budget in the network. 10^4 random matrices are computed with both the observed connectivity matrix and the random -null model-matrix, normalised by DAN postsynaptic budget (middle). Manhattan distance matrices of the observed and the simulated random matrices are calculated, which can then be analyzed statistically. (G) Statistical analysis of mean Manhattan distances of similarity matrices is carried out by comparing the distribution of Manhattan distances in the observed data (red) with the mean of 10^4 simulated matrices (blue). The two distributions are significantly different; $p<0.0001$. Therefore, the organization of DAN input connectivity is not random. (H) Related to Figures 2E and F. Method to determine optimal cluster number for hierarchical connectivity clustering. The heights of the clustering dendrogram links are plotted as a function of the number of clusters in decreasing order. We assessed the differences between neighbouring points to determine a threshold that marks the first merge of the hierarchical clustering between two meaningfully different clusters in this data, producing an optimal cluster number. Here the last two neighbouring points with a greater difference are denoted by red and green dots and the threshold is 0.15. (I) Mantel test to determine statistical significance of correlations between cluster results compared in tanglegrams. Related to Figure 2H. Here morphological DAN data in form of an NBLAST similarity matrix is compared to the observed connectivity distance matrix from (F). Distance matrices are first compared by a Pearson's correlation of the Manhattan distributions. One of the matrices (here the connectivity) is subsequently randomized 10^7 times and the resulting matrices are compared to the observed NBLAST distance. Lastly (right), the correlation coefficients that are higher than the correlation coefficient between the observed data are divided by the number of randomisations (10^7) to obtain a p-value. A small p-value suggests the compared distance matrixes are correlated. (J) A multistep clustering approach to classify DAN input neurons. (Left) Coarse clusters are generated by the average linkage distance of an 'all-by-all' NBLAST comparison of simplified neurons. Neurons are simplified to 1 branchpoint and neurites with a Strahler order <1. This leaves the soma tract as well as the main neurite. This first step works unsupervised on all 821 neurons. Resulting in 20 coarse clusters as shown in Figure (3I). Middle: The average linkage of NBLAST scores is determined between neurons and used for clustering. Means are weighted 80:20 to respect defining neural features. 80 towards the core neurons produced by simplifying neurons down to 3 branch points from the soma, 20 towards the complement of the core neuron - "the fine branches" (green). This

example shows SEZONs which comprise of long tracts and simple branching patterns within the core neuron. This created 153 sub-clusters with little human supervision. (Right) Fine clustering. Neurons in each sub cluster have different key morphological features thus subsequent clustering steps are different in exact parameter settings and weighted means. These settings are reviewed manually to ensure neuron clusters had been sensibly assigned. We determined the step - fine clustering – in most cases to be sufficiently accurate to separate all neurons that are morphologically different in different sub-sub-clusters. Only in a few cases can manual expert review further subdivide these groups of neurons.

Figure S3 related to Figure 3

(A) Full detail of the screen highlighted in Figure 3A. (B) Comparison of localization of postsynapses created in review cycles in addition to normal expert review. Plotting newly added synapses together with existing identified synapses along a PAM DAN dendrite, shows additional tracing of reviewed DANs to create new postsynapses uniformly distributed over the whole dendrite. In addition, plotting the distribution of distances to the root of the dendritic tree confirms that both populations are mixed along the dendrite. This indicates that neurons that have undergone standard expert review, but have not been subject to increased review, can be treated as randomly sampled. (C) MBON activation paired with odor exposure can write memories. Following identification in the screen, MBON-γ5β´2a and MBON-γ4γ5 were re-tested and 30min memory was assessed. CsChrimson mediated activation of MBON-γ5β´2a formed weak but significantly positive memory, whereas MBON-γ4γ5 activation formed significant aversive memory. Asterisks denote $p<0.0021$ (PAM DANs), $p<0.0247$ (MBON-γ5β´2a), and $p<0.026$ (MBON-γ4γ5); one-way ANOVA, with Dunnett's post hoc test for multiple comparisons, n=10. (D) Previous experience reinforcement network for MBON-γ5β´2a and MBON-γ4γ5. Both MBONs receive dendritic input in the γ5 MB compartment but reinforce memories of different valence. MBON-γ4γ5 provides cross compartmental feedback innervating PPL1-γ1pedc but not PAM-γ5 DANs. MBON-γ5β´2a preferentially innervates the γ5 DANs and not PPL1-γ1pedc DANs. Other MBONs like MVP2 (MBON-γ1>αβpedc) might also be involved, but instead of changing valence this MBON provides feed-forward inhibition. (E-I) Related to Figure 3 E and F. Temperature and genetic controls for *Shi*^{ts} block during training with sucrose and DEET reinforcement. (J) SEZON activation with CsChrimson paired with odor followed by testing for 30 min memory replicates the screening phenotypes.

SEZON02 produces aversive memories. Asterisks denote $p<0.0245$ (SEZON02); one-way ANOVA, with Dunnett's post hoc test for multiple comparisons, n=10. (K) Neato layout of a dendrogram of the dendrite of the PPL1-γ1pedc DAN showing position of MBON input. Postsynapses receiving MBON input are highlighted. All MBON input is in the Crepine branches that are closest to the axon. Note: MBON-γ4γ5 is the strongest MBON input. (L) Relates to Figure 3G. Localization of inputs from all our clustered input neurons on the PPL1-γ1pedc DAN dendrite sorted by branches. Input specificity to all branches is evident.

Figure S4 related to Figure 4

(A) Neato dendrograms of two PAM-γ5(fb) DANs with MBON-γ5β´2a synaptic inputs shown in green. In these two PAM-γ5(fb) DANs MBON-γ5β´2a inputs localize close to the root of the dendrite (left) and on a single branch (right). MBON-γ5β´2a contribute the largest fraction of the postsynaptic budget of γ5(fb) DANs..(B) Axon morphology of the PAM DANs is correlated to dendrite connectivity. A tanglegram showing the correlation between morphological clustering of PAM DAN axons and dendritic connectivity clustering (Pearson's Correlation: $r=0.292$; $p=0.00006$, $p_w=0.01$ Mantel test). (C) Corresponds to Figure 4F. Genetic driver controls show extinction phenotypes. Parental lines used in the extinction experiments were crossed to wildtype flies (wt) and heterozygote progeny were tested for extinction learning (n=4). (D) Corresponds to Figure 4G. Permissive temperature control; no defects in 30 min sugar memory were observed (n=6). (E) Corresponds to figure 4G. Parental genetic driver controls for 30 min sugar memory. Parental lines were crossed to wildtype flies (wt) and heterozygote flies were tested for 30 min sucrose memory (n=5-6). (F) Neato dendrogram representation of MBON-γ5β´2a. Postsynapses on the dendrite are marked. Colors correspond to DAN clusters with closest pre-synapse to MBON postsynapses. To account for DA diffusion we allowed a 2 µm radius around the respective postsynapse. Dendritic branches are numbered 1-6 where 1,2, 6 are closest to the root of the dendrite. PAM-γ5fb, -γ5ba, -γ5da, and -β´2a (2) may influence specific branches, with the γ5da and γ5fb DANs being mutually exclusive and the γ5ba and β´2a (2) cluster localizing very close to the root of the dendritic tree. Morphologically distinct PAM DANs that receiving different inputs might therefore reinforce synaptic plasticity at specific branches of the MBON-γ5β´2a dendrite.

Materials and Methods

Neuron reconstruction - 'tracing' in FAFB

Neurons were reconstructed in a serial section transmission electron microscopy (ssTEM) volume of a full adult fly *D. melanogaster* brain (FAFB) [1] using CATMAID, a web-based software for collaborative neural circuit reconstruction from large image datasets (https://catmaid.readthedocs.io/en/stable/) [2, 3]. Consistent with previous studies [3-5], tracing followed the centerline of a neuron's profiles through the dataset to reconstruct neurite morphology and annotate synaptic sites. We used an established and tested iterative approach [3] where initial reconstruction is followed by a systematic proofreading by at least two expert reviewers (>500 h of tracing experience). We also took advantage of recent automatic segmentation efforts of the FAFB dataset [6], where flood-filling algorithms create volumetric segmentations of the EM data. These segmentations are then skeletonised to produce neuron fragments which can be joined together to expedite reconstruction. Human proof-reading is still required to remove incorrect merges of skeletons. In this study auto-segmentation was only used to aid tracing of DAN input neurons to identification (see below).

Synaptic sites were identified based on three, previously described criteria [7] and reviewed as above: an active zone with (1) T-bar(s) and (2) surrounding vesicle cloud, and (3) a synaptic cleft to which all postsynaptic neurons must have access. In *Drosophila*, presynapses have been found on fine axonal processes [3], boutons [8], and other neurites that are neither in the dendritic nor the axonal field. Post-synapses have been found on large or fine dendritic processes and spine-like twigs that are shorter than 3 µm [3]. It has been estimated that the tracing approach employed finds 99.8% of presynapse and 91.7% of postsynapses [3]. The probability of identifying false-positive postsynapses is 2.2% and negligible for presynapses. Reconstructed neurons were visualized using Blender 3D, an open-source 3D software (https://www.blender.org/) or natverse [9] and RCatmaid packages in R (http://jefferis.github.io/rcatmaid/). Neuron data from CATMAID were imported using an existing CATMAID plugin for Blender (https://github.com/ schlegelp/CATMAID-to-Blender [5]).

Identifying, tracing and quality control of DANs

DANs were first identified by selecting potential profiles in the midline commissure between left and right hemisphere MBs. These profiles were traced until axonal branches could be identified in the MB compartment of interest. We exhausted all possible profiles between the two MB compartments and identified all γ5 DANs, both PPL1-γ1pedc DANs and all right hand side (RHS) β´2a DANs. After identification, DANs were traced and reviewed (described above). The RHS PPL1-γ1pedc DAN was completed and 74% reviewed. 20 PAM-γ5 DANs on the RHS and 9 on the left were reconstructed and the RHS neurons were reviewed. 18 PAM-γ5 DANs were reviewed to more than 50% and 7 to more than 97%, reaching an average of 75%. 3 PAM-β´2 DANs were reviewed to 99% and a 4th to 30%. Any neurons that were not reviewed to at least 30% were excluded from the analyses in this study.

We note that it was more difficult to reconstruct DANs than many other neurons in the *Drosophila* brain. DAN dendrites are very thin and have a dark/granular texture which increases the likelihood of missing branches and synapses. We therefore scrutinized completion and postsynapse annotation for 7 PAM-γ5 DANs (representing all morphological clusters), 3 PAM-β´2a DANs and the PPL1-γ1pedc DAN. Following this extended reconstruction effort we are confident that we have annotated 100% of the postsynapses on these selected DANs. Comparing data obtained from the regular review protocol to that from our extended review effort showed that regular review captured ~30% of the postsynapses on more than 60% of all cable. We also analysed the placement of old (regular review) and new (added following extensive review) synapses, by measuring their geodesic (along-the-arbor) distance to the dendritic root (Figure S4B). This analysis showed that each round of additional review randomly adds new synapses all along the arbor.

Tracing Dendritic Inputs

When a postsynapse was annotated on a DAN, a single-(seminal) node profile was placed in the centre of the presynaptic cell, unless a neuron or fragment was already present. To reconstruct upstream neurons from these seminal nodes we randomised the sampling order from each postsynapse within the total population on a neuron-by-neuron basis (Figure S3). For the reviewed PAM DANs (18 γ5 and 4 β´2a) we traced over 90% of the input profiles to identified postsynapses. For the PPL1-γ1pedc, we traced 50% of the inputs to identified postsynapses. Tracing inputs to this collection of DAN postsynapses recovered 821 upstream neurons, some of which are connected to multiple DANs. The tracing of these upstream neurons varies in level of completeness. However all neurons are traced to at least a microtubule

containing backbone and were followed to a soma to retrieve their gross morphologies.

Analysis of neuroanatomical features

Resources

All analyses were performed in R and Python using open-source software. PyMaid (https://github.com/schlegelp/PyMaid) and RCatmaid (http://jefferis.github.io/rcatmaid/; http://jefferis.github.io/elmr/) were used to interface with CATMAID servers and perform morphological analyses. Hierarchical clustering was performed using base R functions and dendrogram visualisations with dendroextras (https://github.com/jefferis/dendroextras). Tanglegrams were generated using dendextend (https://github.com/talgalili/dendextend) [10]. Mantel tests used the vegan R package (https://github.com/vegandevs/vegan). Neuron analyses were performed with natverse functionality (https://github.com/natverse/nat) [9] or custom-written code, which is available on request.

PAM DAN clustering by morphology

To compensate for different levels of tracing completeness, DANs were simplified to their longest tree with 200 branch points (the minimum number of branch points throughout the PAM DAN population). Morphological similarity matrices were calculated using NBLAST [11]. Hierarchical clustering was performed using base R functions, taking Euclidean distance matrices of similarity scoring, with average linkage clustering criterion.

DAN PPL-γ1pedc postsynapse clustering

For PPL1-γ1pedc the x, y and z coordinates of postsynapses on the dendrite were clustered using Ward's hierarchical clustering in the SciPy package (https://www.scipy.org/, [12]). The elbow method (Figure S1H) validated the number of clusters and the segregation of PPL1-γ1pedc's dendritic tree into 4 separate areas.

Neuropil of origin

To identify SEZONs and LH-associated neurons, the cable length within the respective neuropil mesh (3D bounding box) was calculated. A cut off of >60 nodes was required for classification.

Input morphology clustering (specified in Figure S2J)

Morphology clustering of all upstream neurons was performed using hierarchical clustering with average linkage criterion. This involved a multi-step approach to account for varying levels of tracing and for the morphological diversity of 821 neurons. Coarse clustering was performed taking the soma tract as the primary feature of neuron identity. Subsequently the larger primary clusters were subclustered by splitting neurons into the primary neurite and its complement/remainder. Similarity matrices were calculated using NBLAST and an element-wise mean (80:20) was used for clustering. For fine clusters, weighting methods were selected iteratively depending on overall sub-cluster morphology,

Dendrogram representations

Dendrogram representations were created as in [13]. Dendrograms are 2D representations of 3D neuronal reconstructions which preserve the topology of neuron and visualise specific synapses on specific branches. Code available (https://github.com/markuspleijzier/AdultEM/tree/master/Dendrogram_code) using the Graphviz library (https://graphviz.gitlab.io/ [14]) via Python bindings provided by NetworkX, (https://networkx.github.io/ [15]).

Marking MBON postsynapses on dendrograms by closest DAN cluster

Euclidean distances between MBON-γ5β´2a postsynapses and the closest DAN presynapse were measured and marked by the identity of the morphological DAN clusters (Figure 1). Then, the Euclidean distances were then thresholded to 2 µm and the synapses below that certain threshold were plotted on a neato dendrogram. Thus, the plot shows all postsynapses within 2 µm diffusion distance from a dopaminergic presynapse.

Analyses of Neuron Connectivity

Edge weight distribution

Edge weight distributions describe how many upstream neurons contribute a given number of presynapses to a connection with a postsynaptic neuron (number of synapses vs frequency). Normalising by the total number of postsynapses details the percentage of the total postsynaptic budget a given number of synapses represents.

For example, if a neuron makes 10 presynapses onto a postsynaptic neuron, which has a total of 100 postsynapses, then that upstream neuron contributes 10% of the postsynaptic budget.

Connectivity clustering

Connectivity information between neurons was retrieved from CATMAID after tracing and annotating synapses. For DAN-connectivity analyses, only neurons upstream of the dendritic region of DANs with > 50 sampled profiles were considered. The number of synapses between DANs and upstream partners was normalized by the number of all traced upstream profiles of the given DAN. Hierarchical clustering was performed by using the Euclidean distance between upstream neurons using Ward's clustering criterion. Connectivity matrix columns were normalised for each DAN. To choose an appropriate number of clusters, a modified version of the elbow method was employed (compare to Figure S2). For DAN-MBON direct connectivity analysis, identified MBONs were collapsed by type. The number of synapses between DANs and MBONs was normalized by the number of all DAN-MBON connections of the given DAN. Hierarchical clustering was performed as described above. Connectivity matrices can be calculated for single branches of a neuron after defining the relevant branchpoints in CATMAID. For the PPL1-γ1pedc DAN, we manually split the dendrite into 4 postsynaptic clusters, as defined in cluster analyses described above, and recorded the specific connectivity to each of these clusters/branches.

DAN connectivity similarity matrices

A connectivity similarity score between 2 DANs was defined as one minus half of the Manhattan distance between their normalised connectivity patterns (normalised connectivity patterns of DANs shown in Figure 2E).

Statistical analysis of DAN connectivity - comparison to a null model of random connectivity

A DAN input connectivity matrix was first randomised 10^4 times, respecting both DAN postsynaptic budget and input neuron presynaptic budget, so that after randomization each row sum and each column sum remained the same as in the observed data (i.e. each DAN gets the same number of inputs and each input neuron has the same number of outputs). Then the Manhattan distance between neurons in the observed data and that in simulated random matrices were calculated and means of these distances were compared to obtain a p-value describing the similarity of

these means. A p-value lower than the significance level concluded that the null model of randomized connectivity could be rejected.

Tanglegrams to compare clustering of 2 feature spaces

Tanglegrams were generated to visually compare morphology and connectivity dendrograms. Following dendextend [10] optimal dendrogram layouts were determined to minimise edge crossing, and minimise L1 norm distance between the corresponding DANs.

Mantel test to determine dependence of 2 feature spaces (as compared in tanglegrams, Figure S2I)

The Mantel test was used to compare 2 sample spaces - here neuron morphology distance matrices obtained from all-by-all NBLAST and distances obtained from connectivity clustering were used. To create distance matrices for connectivity, connectivity matrices were normalized to respect the postsynaptic budget of each downstream neuron - DANs, and the presynaptic budget of any input neuron. The implementation of the Mantel test was based on [16]. Pearson's correlation between the two observed datasets was calculated, then one of the matrices was shuffled 10^7 times and each event tested for correlation with the observed data repeatedly. The number of events where the correlation is higher than between the two original datasets was divided by the amount of comparisons (10^7) to create a p-value. When p-values were lower than the significance level, it was concluded that the null model of independence between the two feature spaces could be rejected.

Matching genetic driver lines to EM skeletons

EM skeletons were matched to published library GAL4 lines using registered Janelia FlyLight micrograph data from VirtualFlyBrain (https://v2.virtualflybrain.org). NBLAST similarity matrices were calculated comparing both data types and top hits were visualised and manually cross compared. In case of new split-GAL4 SS lines created by Masayoshi Ito (Ito et al., in prep), imaging stacks were newly registered with bridging and mirror registrations from the natverse package [9].

Behavioural experiments

All *Drosophila* strains were raised at 25˚C on standard cornmeal-agar food at 50-60% relative humidity in a 12:12 h light:dark cycle. For experiments, female flies bearing effector transgenes were crossed to male flies bearing GAL4 drivers. For driver line details see Key Resources Table. Driver lines were obtained from the

Janelia FlyLight collection [17] or split-GAL4 [18] collections, the Vienna Tiles Project [19], and the InSITE collection [20]. New split-GAL4 'SS' lines were created in the Ito/Rubin labs (Ito et al., in prep). UAS-*CsChrimson* [21] and *UAS-Shibire*^{ts} [22] effectors were used to stimulate and block specific neurons. For wildtype controls Canton-S flies were used. For heterozygous controls, GAL4 lines were crossed to Canton-S flies.

The odors used for US substitution, sucrose learning and DEET learning experiments were 10^{-3} dilutions of 3-octanol (OCT) and 4-methylcyclohexanol (MCH) in mineral oil. For extinction experiments odor concentrations of 10^{-6} were used to avoid pre-exposure effects [13]. Experiments were performed at 23˚C and 55-65% relative humidity, except for electric shock learning which occurred at 70% relative humidity.

US-substitution experiments using CsChrimson

In both the behavioural screen and follow-up experiments, neurons were artificially activated to substitute for an unconditioned stimulus in the training chamber of a T-maze. Prior to the experiments, 80-120 1-5 day old mixed sex flies were housed on standard food supplemented with 1% all-trans-Retinal for 3 days before a 20 – 28 h starvation period in vials containing 2 ml 1% agar as a water source and a 2x4 cm strip of Whatman filter paper. During training, groups of flies were exposed to the CS- for 2 min followed by 30 s rest with fresh air, then 2 min of CS+ odor with optogenetic activation of the genetically encoded Channel Rhodopsin with red light exposure. LEDs were set to 500Hz. For screening, immediate memory testing followed. Flies were transferred back into their starvation vials after training before testing 30 min memory.

Appetitive olfactory learning with sucrose reward

Prior to the experiments, 80-120 3-8 day old mixed sex flies were starved for 20-28 h in vials containing 2 ml 1% agar as a water source and a 2x4 cm strip of Whatman filter. Flies were transferred to 32 ˚C 30 min before training. During training, groups of flies were exposed to the CS- odor with dry paper for 2 min followed by 30 s of fresh air, then 2 min of CS+ odor exposure with dry sugar paper. Flies were either tested immediately after training or were transferred back into 25˚C starvation vials after training prior to testing 30 min memory.

Aversive olfactory learning with bitter reinforcement

Flies were aversively trained with DEET as previously described [23]. In brief, prior 80-120 3-7 day old mixed sex flies were starved for 20-24 h in vials containing 2 ml 1% agar and a 2x4 cm strip of Whatman filter paper. Training and immediate testing were performed at 32˚C. During training groups of flies were exposed to the CS- odor with 1% agar on filter paper for 2 min followed by 30 s fresh air, then 2 min of CS+ odor with 0.4% DEET, 3 M xylose and 100 mM sucrose in 1% agar on filter paper. Flies were tested for their odor preference immediately after training.

Aversive memory extinction

Extinction memory was tested as described [13]. In brief, mixed sex groups of 80-120 flies were transferred into vials with 2 ml cornmeal medium and a 2x4 cm strip of Whatman paper for 18-26 h before training. Aversive olfactory conditioning in the T-maze was conducted as previously described [24]. Flies were exposed to the CS+ odor for 1 min paired with twelve 90 V electric shocks at 5 s intervals. Following 45 s of clean air, the CS- odor was presented for 1 min without shock. Immediately after training flies were transferred to 32˚C. 30 min later flies were re-exposed twice to either the CS- or CS+ odor with a 15 min interval. Flies were then returned to permissive 23˚C and tested 15 min later for memory performance.

Memory testing and statistical analyses of behavioural data

To test memory performance flies were loaded into the T-maze and transported to the choice point where they were given two min to choose between the CS+ and CS- odors in the dark. A Performance Index was calculated as the number of flies in the CS+ arm minus the number in the CS- arm, divided by the total number of flies [23]. MCH and OCT, were alternately used as CS+ or CS- and a single sample, or n, represents the average performance score from two reciprocally trained groups. Statistical analysis was carried out with GraphPad, Prism (v8.1). All experiments were analysed with a one-way ANOVA. For extinction CS- re-exposure flies were compared with CS+ re-exposure flies and Tukey's post-doc analyses for multiple comparisons applied. For all other experiments statistical comparisons were performed between a wildtype control and Dunnett's post hoc analysis carried out for multiple comparisons.

Key Resources Tables

Chemicals		
Sucrose	Sigma-Aldrich	Cat# S0389
Mineral Oil	Sigma-Aldrich	Cat#M5904
4-methylcyclohexanol (98%)	Sigma-Aldrich	Cat#218405
3-octanol (99%)	Sigma-Aldrich	Cat#153095
Retinal	Sigma-Aldrich	Cat#R2500
DEET	Sigma-Aldrich	Cat#36542
Xylose	Sigma-Aldrich	Cat#X1500

Experimental Models: Organisms/Strains		
Drosophila: Canton-S	Waddell Lab	
Drosophila: R58E02-GAL4	Bloomington Drosophila Stock Center; FlyLight [17]	RRID:BDSC_41347
Drosophila: MB504B-GAL4	Bloomington Drosophila Stock Center FlyLight [17]	RRID:BDSC_68329
Drosophila: MB315C-GAL4	Bloomington Drosophila Stock Center FlyLight [17]	RRID:BDSC_68316
Drosophila: MB320C-GAL4	Bloomington Drosophila Stock Center FlyLight [17]	RRID:BDSC_68253
Drosophila: 0273-GAL4	InSITE collection [20]	Waddell lab
Drosophila: MB077B-GAL4	Bloomington Drosophila Stock Center FlyLight [17]	RRID:BDSC_68283
Drosophila: VT006202-GAL4	Vienna Tiles Project [19]	RRID:BDSC_72445
Drosophila: 0104-GAL4	InSITE collection [20]	RRID:BDSC_62639
Drosophila: 0804-GAL4	InSITE collection [20]	RRID:BDSC_6325
R48B04-GAL80; 0104-GAL4	[17, 20]	Waddell lab
Drosophila: GMR88F08-GAL4	Bloomington Drosophila Stock Center; FlyLight [17]	RRID:BDSC_47982
Drosophila: GMR88E01-GAL4	Bloomington Drosophila Stock Center; FlyLight [17]	RRID:BDSC_48397
Drosophila: GMR66C08-GAL4	Bloomington Drosophila Stock Center; FlyLight [17]	RRID:BDSC 49412
Drosophila: GMR48B04-GAL4	Bloomington Drosophila Stock Center; FlyLight [17]	RRID:BDSC_50347
Drosophila: GMR87A01-GAL4	Bloomington Drosophila Stock Center; FlyLight [17]	RRID:BDSC_40472
Drosophila: SS46348-GAL4	Ito/Rubin labs	Ito et al, in prep

Drosophila: SS28305-GAL4	Ito/Rubin labs	Ito et al, in prep
Drosophila: SS27959-GAL4	Ito/Rubin labs	Ito et al, in prep
Drosophila: SS52050-GAL4	Ito/Rubin labs	Ito et al, in prep
Drosophila: SS45245-GAL4	Ito/Rubin labs	Ito et al, in prep
Drosophila: SS45251-GAL4	Ito/Rubin labs	Ito et al, in prep
Drosophila: SS52046-GAL4	Ito/Rubin labs	Ito et al, in prep
Drosophila: S49970-GAL4	Ito/Rubin labs	Ito et al, in prep
Drosophila: SS45221-GAL4	Ito/Rubin labs	Ito et al, in prep
Drosophila: SS47568-GAL4	Ito/Rubin labs	Ito et al, in prep
Drosophila: SS49941-GAL4	Ito/Rubin labs	Ito et al, in prep
Drosophila: SS39616-GAL4	Ito/Rubin labs	Ito et al, in prep
Drosophila: SS27580-GAL4	Ito/Rubin labs	Ito et al, in prep
Drosophila: SS28308-GAL4	Ito/Rubin labs	Ito et al, in prep
Drosophila: SS21077-GAL4	Ito/Rubin labs	Ito et al, in prep
Drosophila: SS45222-GAL4	Ito/Rubin labs	Ito et al, in prep
Drosophila: SS42968-GAL4	Ito/Rubin labs	Ito et al, in prep
Drosophila: SS46613-GAL4	Ito/Rubin labs	Ito et al, in prep
Drosophila: SS35902-GAL4	Ito/Rubin labs	Ito et al, in prep
Drosophila: SS51316-GAL4	Ito/Rubin labs	Ito et al, in prep
Drosophila: SS31522-GAL4	Ito/Rubin labs	Ito et al, in prep
Drosophila: SS21206-GAL4	Ito/Rubin labs	Ito et al, in prep
Drosophila: SS31827-GAL4	Ito/Rubin labs	Ito et al, in prep
Drosophila: SS39070-GAL4	Ito/Rubin labs	Ito et al, in prep
Drosophila: SS25028-GAL4	Ito/Rubin labs	Ito et al, in prep
Drosophila: SS24588-GAL4	Ito/Rubin labs	Ito et al, in prep
Drosophila: SS27978-GAL4	Ito/Rubin labs	Ito et al, in prep
Drosophila: SS46337-GAL4	Ito/Rubin labs	Ito et al, in prep
Drosophila: SS32768-GAL4	Ito/Rubin labs	Ito et al, in prep
Drosophila: SS36651-GAL4	Ito/Rubin labs	Ito et al, in prep
Drosophila: SS46596-GAL4	Ito/Rubin labs	Ito et al, in prep
Drosophila: SS42983-GAL4	Ito/Rubin labs	Ito et al, in prep
Drosophila: SS24252-GAL4	Ito/Rubin labs	Ito et al, in prep
Drosophila: SS21208-GAL4	Ito/Rubin labs	Ito et al, in prep
Drosophila: SS32151-GAL4	Ito/Rubin labs	Ito et al, in prep
Drosophila: LH991-GAL4	Jefferis Lab [25]	NA
Drosophila: LH2241-GAL4	Jefferis Lab [25]	NA
Drosophila: LH989-GAL4	Jefferis Lab [25]	NA
Drosophila: LH1395-GAL4	Jefferis Lab [25]	NA
Drosophila: LH2278-GAL4	Jefferis Lab [25]	NA

Drosophila: LH1538-GAL4	Jefferis Lab [25]	NA
Drosophila: LH1539-GAL4	Jefferis Lab [25]	NA
Drosophila: LH1396-GAL4	Jefferis Lab [25]	NA
Drosophila: UAS-*Shibire*^{ts1}	Kitamoto 2001	RRID:BDSC_44222
Drosophila: UAS-CsChrimson.mVenus	Bloomington Drosophila Stock Center [21]	RRID:BDSC_55135 RRID:BDSC_55136

Reagent or Resource	**Source**	**Identifier**
Antibodies		
Anti-GFP	Abcam	RRID: AB_300798
DsRed Polyclonal	Sigma-Aldrich	Cat#S7653
nc82	DSHB	AB_2314866

Software		
Blender 3D	Blender Online Community	https://www.blender.org/
Natverse	[9]	https://github.com/natverse/nat/
Dendroextras	[10]	https://github.com/jefferis/dendroextras/
R	R Development Core Team	http://www.R-project.org/
catmaidR	Jefferis and Cardona labs	http://jefferis.github.io/rcatmaid/
CATMAID	[2, 3]	https://catmaid.readthedocs.io/en/stable/index.html#
Python	Python Software Foundation	https://www.python.org/
PyMaid	Philipp Schlegel	https://github.com/schlegelp/PyMaid
Dendrogram code	Markus Pleijzier	https://github.com/markuspleijzier/AdultEM/tree/master/Dendrogram_code
Graphviz	[14]	https://www.graphviz.org
NetworkX	[15]	https://networkx.github.io/
Dendextend	[10]	https://github.com/jefferis/dendroextras
Fiji	NIH [26]	http://fiji.sc/
GraphPad Prism 6	GraphPad Software, La Jolla, CA	https://www.graphpad.com/ scientific-software/prism/
Adobe Illustrator CC	Adobe Systems, San Jose, CA	https://www.adobe.com/uk/products/illustrator.html

Supplemental References

1. Zheng, Z., Lauritzen, J.S., Perlman, E., Robinson, C.G., Nichols, M., Milkie, D., Torrens, O., Price, J., Fisher, C.B., Sharifi, N. et al. (2018). A Complete Electron Microscopy Volume of the Brain of Adult Drosophila melanogaster. Cell. *174*, 730-743.
2. Saalfeld, S., Cardona, A., Hartenstein, V., and Tomancak, P. (2009). CATMAID: collaborative annotation toolkit for massive amounts of image data. Bioinformatics. *25*, 1984-1986.
3. Schneider-Mizell, C.M., Gerhard, S., Longair, M., Kazimiers, T., Li, F., Zwart, M.F., Champion, A., Midgley, F.M., Fetter, R.D., Saalfeld, S. et al. (2016). Quantitative neuroanatomy for connectomics in Drosophila. Elife. *5*, pii: e12059. doi: 10.7554/eLife.12059.
4. Eichler, K., Li, F., Litwin-Kumar, A., Park, Y., Andrade, I., Schneider-Mizell, C.M., Saumweber, T., Huser, A., Eschbach, C., Gerber, B. et al. (2017). The complete connectome of a learning and memory centre in an insect brain. Nature. *548*, 175-182.
5. Schlegel, P., Texada, M.J., Miroschnikow, A., Schoofs, A., Huckesfeld, S., Peters, M., Schneider-Mizell, C.M., Lacin, H., Li, F., Fetter, R.D. et al. (2016). Synaptic transmission parallels neuromodulation in a central food-intake circuit. Elife. *5*, pii: e16799. doi: 10.7554/eLife.16799.
6. Li, P.H., Lindsey, L.F., Januszewski, M., Zheng, Z., Bates, A.S., Taisz, I., Tyka, M., Nichols, M., Li, F., Perlman, E. et al. (2019). Automated Reconstruction of a Serial-Section EM Drosophila Brain with Flood-Filling Networks and Local Realignment. bioRxiv. 605634.
7. Prokop, A., and Meinertzhagen, I.A. (2006). Development and structure of synaptic contacts in Drosophila. Semin Cell Dev Biol. *17*, 20-30.
8. Butcher, N.J., Friedrich, A.B., Lu, Z., Tanimoto, H., and Meinertzhagen, I.A. (2012). Different classes of input and output neurons reveal new features in microglomeruli of the adult Drosophila mushroom body calyx. J Comp Neurol. *520*, 2185-2201.
9. Bates, A.S., Manton, J.D., Jagannathan, S.R., Costa, M., Schlegel, P., Rohlfing, T., and Jefferis, G.S.X.E. (2019). The natverse: a versatile computational toolbox to combine and analyse neuroanatomical data. bioRxiv. 006353.
10. Galili, T. (2015). dendextend: an R package for visualizing, adjusting, and

comparing trees of hierarchical clustering. Bioinformatics. *31*, 3718-3720.

11. Costa, M., Manton, J.D., Ostrovsky, A.D., Prohaska, S., and Jefferis, G.S. (2016). NBLAST: Rapid, Sensitive Comparison of Neuronal Structure and Construction of Neuron Family Databases. Neuron. *91*, 293-311.
12. Virtanen, P., Gommers, R., Oliphant, T.E., Haberland, M., Reddy, T., Cournapeau, D., Burovski, E., Peterson, P., Weckesser, W., Bright, J. et al. (2020). SciPy 1.0: fundamental algorithms for scientific computing in Python. Nat Methods. https://doi.org/10.1038/s41592-019-0686-2
13. Felsenberg, J., Jacob, P.F., Walker, T., Barnstedt, O., Edmondson-Stait, A.J., Pleijzier, M.W., Otto, N., Schlegel, P., Sharifi, N., Perisse, E. et al. (2018). Integration of Parallel Opposing Memories Underlies Memory Extinction. Cell. *175*, 709-722.
14. Ellson, J., Gansner, E., Koutsofios, L., North, S.C., and Woodhull, G. (2002). Graphviz— Open Source Graph Drawing Tools Graph Drawing. 483-484.
15. Hagberg, A. A., Schult, D. A. and Swart, P. J. (2008). Exploring network structure, dynamics, and function using networkX. Proceedings of the 7th Python in Science Conference (SciPy20008). Pasadena, CA, pp11-15.
16. Legendre, P., and Legendre, L. (2012). Numerical Ecology. 3rd English Edition.
17. Jenett, A., Rubin, G.M., Ngo, T.T., Shepherd, D., Murphy, C., Dionne, H., Pfeiffer, B.D., Cavallaro, A., Hall, D., Jeter, J. et al. (2012). A GAL4-driver line resource for Drosophila neurobiology. Cell Rep. *2*, 991-1001.
18. Luan, H., Peabody, N.C., Vinson, C.R., and White, B.H. (2006). Refined spatial manipulation of neuronal function by combinatorial restriction of transgene expression. Neuron. *52*, 425-436.
19. Tirian, L., and Dickson, B.J. (2017). The VT GAL4, LexA, and split-GAL4 driver line collections for targeted expression in the Drosophila nervous system. bioRxiv. 198648.
20. Gohl, D.M., Silies, M.A., Gao, X.J., Bhalerao, S., Luongo, F.J., Lin, C.C., Potter, C.J., and Clandinin, T.R. (2011). A versatile in vivo system for directed dissection of gene expression patterns. Nat Methods. *8*, 231-237.
21. Klapoetke, N.C., Murata, Y., Kim, S.S., Pulver, S.R., Birdsey-Benson, A., Cho, Y.K., Morimoto, T.K., Chuong, A.S., Carpenter, E.J., Tian, Z. et al. (2014). Independent optical excitation of distinct neural populations. Nat Methods. *11*, 338-346.
22. Kitamoto, T. (2001). Conditional modification of behavior in Drosophila by targeted expression of a temperature-sensitive shibire allele in defined neurons. J Neurobiol. *47*, 81-92.

23. Das, G., Klappenbach, M., Vrontou, E., Perisse, E., Clark, C.M., Burke, C.J., and Waddell, S. (2014). Drosophila learn opposing components of a compound food stimulus. Curr Biol. *24*, 1723-1730.
24. Tully, T., and Quinn, W.G. (1985). Classical conditioning and retention in normal and mutant Drosophila melanogaster. J Comp Physiol [A]. *157*, 263-277.
25. Dolan M-J., Belliart-Gue'rin, Bates A.S.,Frechter S., Lampin-Saint-Amaux A., Aso Y., Roberts R.J.V., Schlegel P., Wong A., Hammad A., Bock D.D., Rubin G.M., Preat T., Placais P-Y., and Jefferis G.S.X.E. (2018). Communication from Learned to Innate Olfactory Processing Centers Is Required for Memory Retrieval in Drosophila. Neuron 100, 651–668.
26. Schindelin, J., Arganda-Carreras, I., Frise, E., Kaynig, V., Longair, M., Pietzsch, T., Preibisch, S., Rueden, C., Saalfeld, S., Schmid, B. et al. (2012). Fiji: an open-source platform for biological-image analysis. Nat Methods. *9*, 676-682.

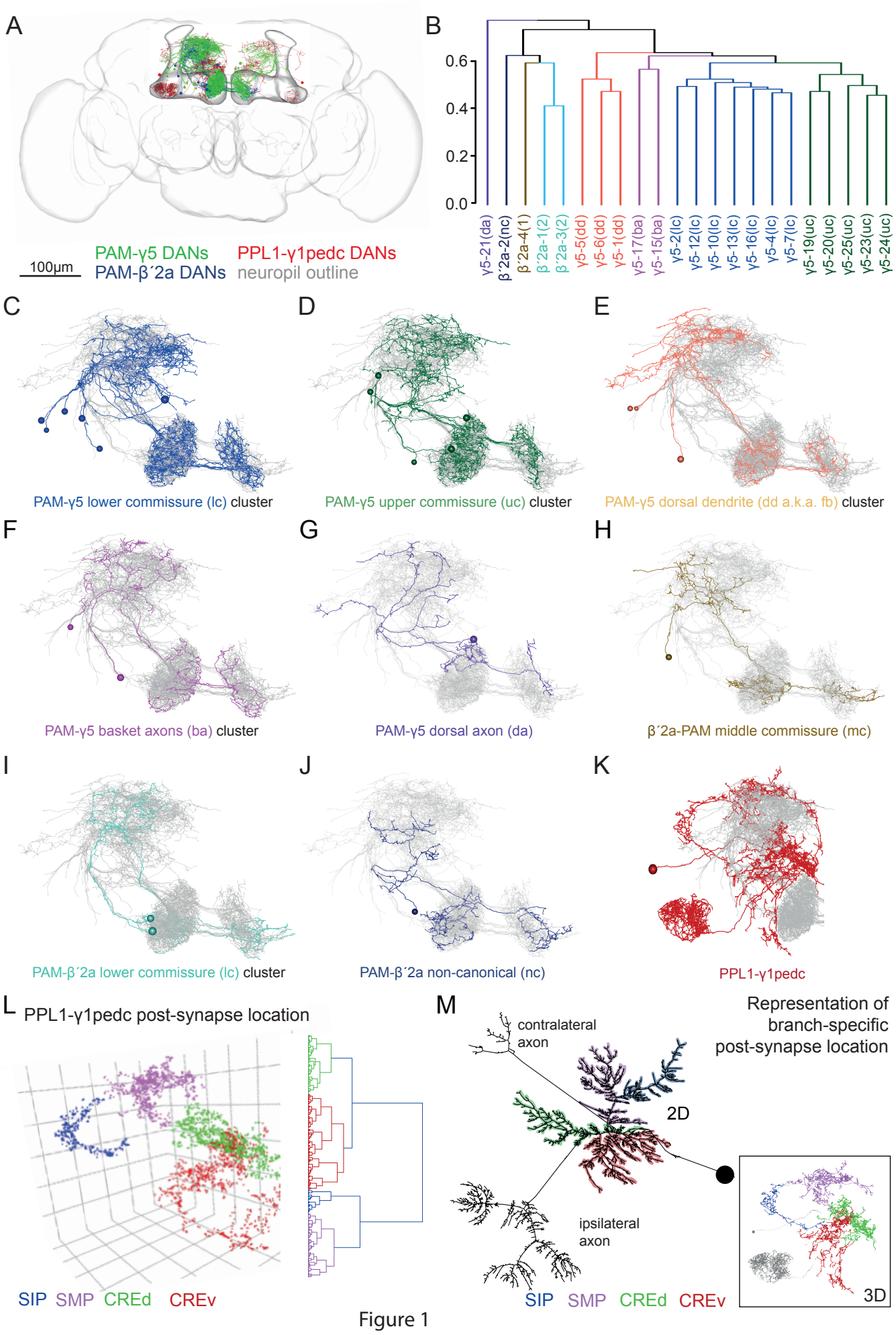
A
100µm
PAM-γ5 DANs
PAM-β´2a DANs
PPL1-γ1pedc DANs
neuropil outline
B
0.6
0.4
0.2
0.0
γ5-21(da)
β´2a-2(nc)
β´2a-4(1)
β´2a-1(2)
β´2a-3(2)
γ5-5(dd)
γ5-6(dd)
γ5-1(dd)
γ5-17(ba)
γ5-15(ba)
γ5-2(lc)
γ5-12(lc)
γ5-10(lc)
γ5-13(lc)
γ5-16(lc)
γ5-4(lc)
γ5-7(lc)
γ5-19(uc)
γ5-20(uc)
γ5-25(uc)
γ5-23(uc)
γ5-24(uc)
C
PAM-γ5 lower commissure (lc) cluster
D
PAM-γ5 upper commissure (uc) cluster
E
PAM-γ5 dorsal dendrite (dd a.k.a. fb) cluster
F
PAM-γ5 basket axons (ba) cluster
G
PAM-γ5 dorsal axon (da)
H
β´2a-PAM middle commissure (mc)
I
PAM-β´2a lower commissure (lc) cluster
J
PAM-β´2a non-canonical (nc)
K
PPL1-γ1pedc
L
PPL1-γ1pedc post-synapse location
SIP SMP CREd CREv
M
Representation of branch-specific post-synapse location
contralateral axon
2D
ipsilateral axon
SIP SMP CREd CREv
3D

Figure 1

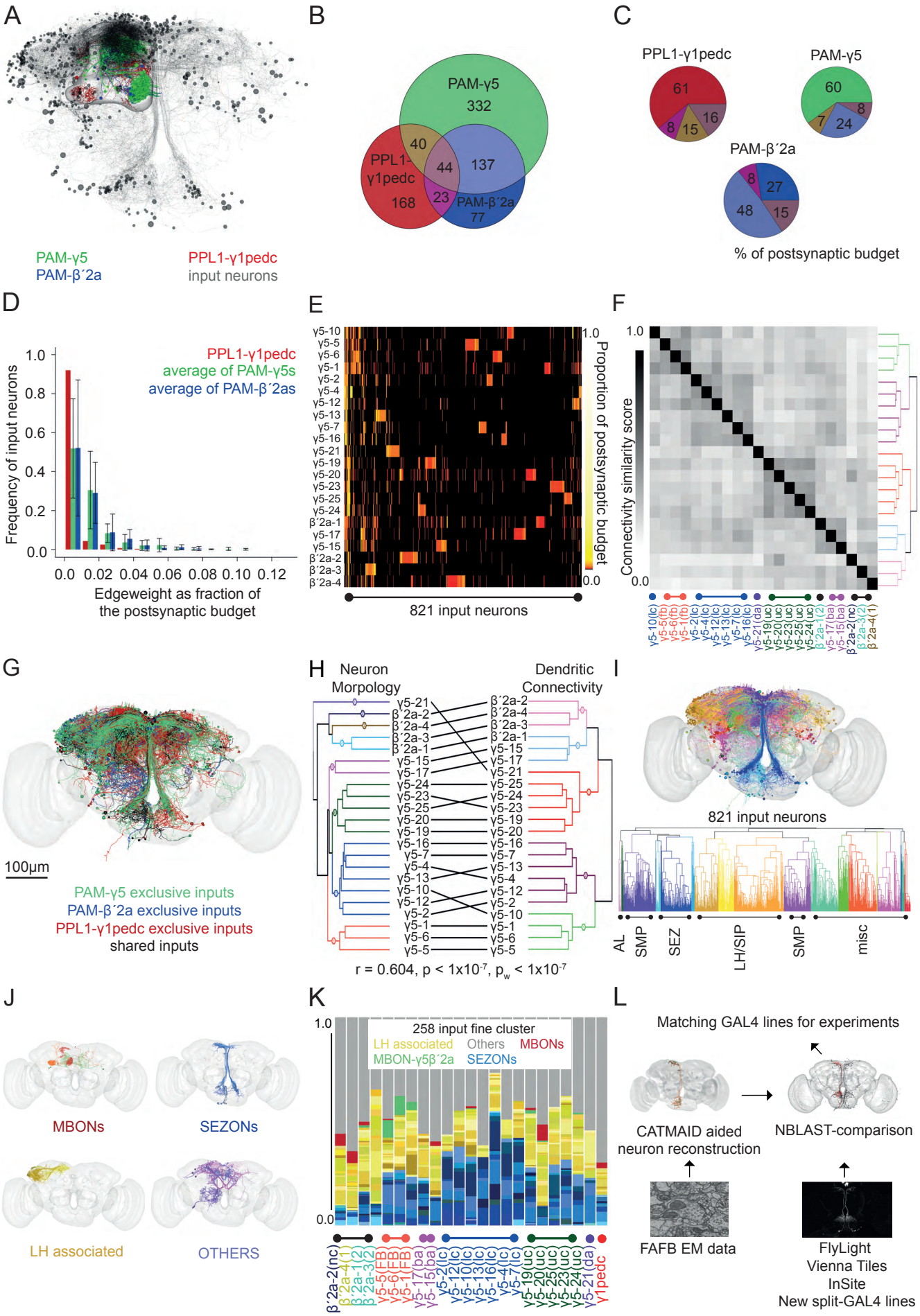
A
PAM-γ5
PAM-β´2a
PPL1-γ1pedc
input neurons
B
PAM-γ5
332
PPL1-γ1pedc
168
PAM-β´2a
77
40
44
137
23
C
PPL1-γ1pedc
61
16
8
15
PAM-γ5
60
8
7
24
PAM-β´2a
8
27
48
15
% of postsynaptic budget
D
PPL1-γ1pedc
average of PAM-γ5s
average of PAM-β´2as
Frequency of input neurons
1.0
0.8
0.6
0.4
0.2
0.0
0.0 0.02 0.04 0.06 0.08 0.10 0.12
Edgeweight as fraction of
the postsynaptic budget
E
γ5-10
γ5-5
γ5-6
γ5-1
γ5-2
γ5-4
γ5-12
γ5-13
γ5-7
γ5-16
γ5-21
γ5-19
γ5-20
γ5-23
γ5-25
γ5-24
β´2a-1
γ5-17
γ5-15
β´2a-2
β´2a-3
β´2a-4
1.0
Proportion of postsynaptic budget
0.0
821 input neurons
F
1.0
Connectivity similarity score
0.0
γ5-10(lc)
γ5-5(fb)
γ5-6(fb)
γ5-1(fb)
γ5-2(lc)
γ5-4(lc)
γ5-12(lc)
γ5-13(lc)
γ5-7(lc)
γ5-16(lc)
γ5-21(da)
γ5-19(uc)
γ5-20(uc)
γ5-23(uc)
γ5-25(uc)
γ5-24(uc)
β´2a-1(2)
γ5-17(ba)
γ5-15(ba)
β´2a-2(nc)
β´2a-3(2)
β´2a-4(1)
G
100µm
PAM-γ5 exclusive inputs
PAM-β´2a exclusive inputs
PPL1-γ1pedc exclusive inputs
shared inputs
H
Neuron
Morpology
Dendritic
Connectivity
γ5-21
β´2a-2
β´2a-4
β´2a-3
β´2a-1
γ5-15
γ5-17
γ5-24
γ5-23
γ5-25
γ5-20
γ5-19
γ5-16
γ5-7
γ5-4
γ5-13
γ5-10
γ5-12
γ5-2
γ5-1
γ5-6
γ5-5
β´2a-2
β´2a-4
β´2a-3
β´2a-1
γ5-15
γ5-17
γ5-21
γ5-25
γ5-24
γ5-23
γ5-19
γ5-20
γ5-16
γ5-7
γ5-13
γ5-4
γ5-12
γ5-2
γ5-10
γ5-1
γ5-6
γ5-5
r = 0.604, p < 1x10-7, pw < 1x10-7
I
821 input neurons
AL
SMP
SEZ
LH/SIP
SMP
misc
J
MBONs
SEZONs
LH associated
OTHERS
K
258 input fine cluster
LH associated
Others
MBONs
MBON-γ5β´2a
SEZONs
1.0
0.0
β´2a-2(nc)
β´2a-4(1)
β´2a-1(2)
β´2a-3(2)
γ5-5(FB)
γ5-6(FB)
γ5-1(FB)
γ5-17(ba)
γ5-15(ba)
γ5-2(lc)
γ5-12(lc)
γ5-10(lc)
γ5-13(lc)
γ5-16(lc)
γ5-4(lc)
γ5-7(lc)
γ5-19(uc)
γ5-20(uc)
γ5-25(uc)
γ5-23(uc)
γ5-24(uc)
γ5-21(da)
γ1pedc
L
Matching GAL4 lines for experiments
CATMAID aided
neuron reconstruction
NBLAST-comparison
FAFB EM data
FlyLight
Vienna Tiles
InSite
New split-GAL4 lines

Figure 2

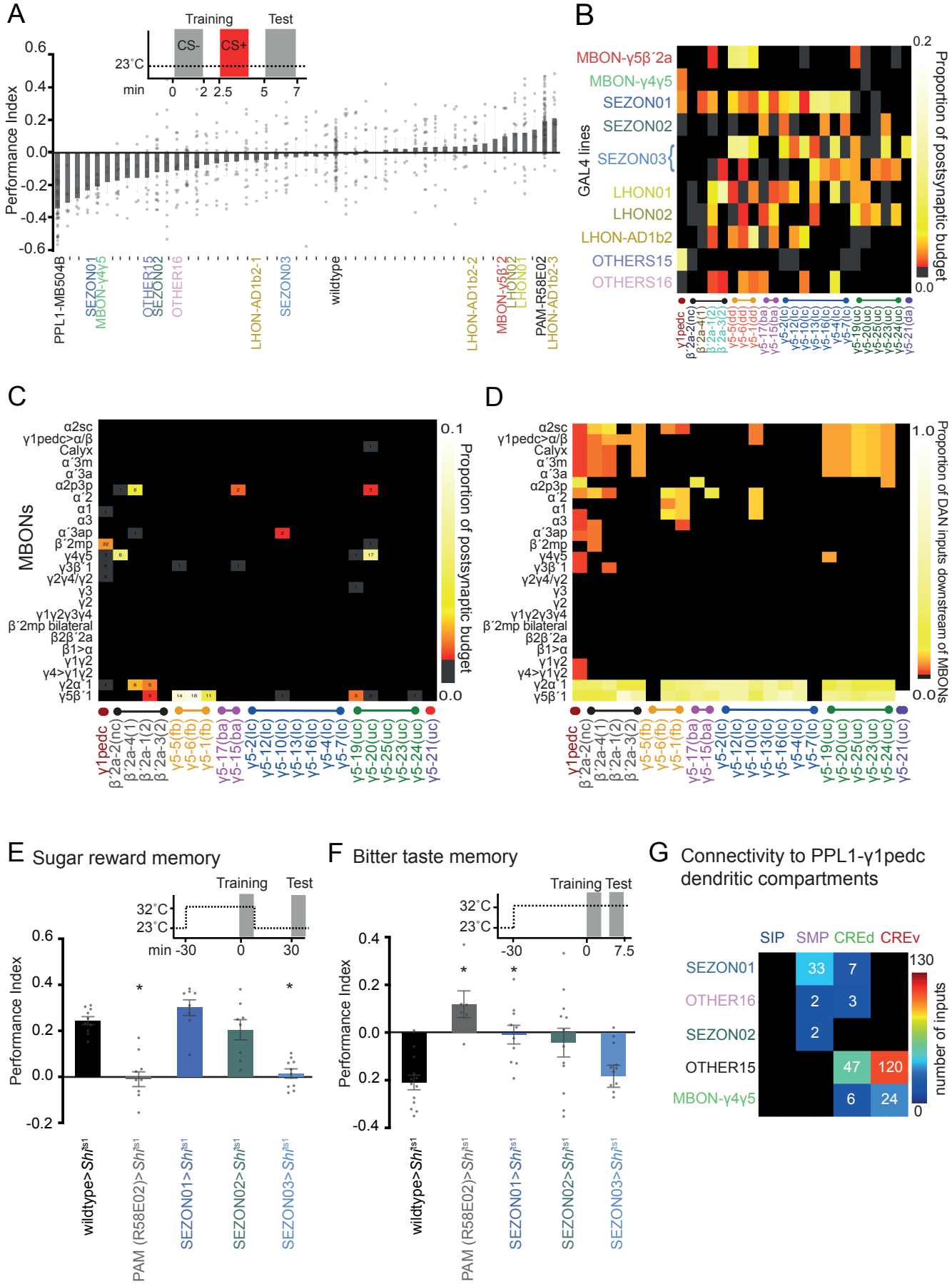
A
Training
Test
CS-
CS+
23°C
min
0
2
2.5
5
7
Performance Index
0.6
0.4
0.2
0.0
-0.2
-0.4
-0.6
PPL1-MB504B
SEZON01
MBON-γ4γ5
OTHER15
SEZON02
OTHER16
LHON-AD1b2-1
SEZON03
wildtype
LHON-AD1b2-2
MBON-γ5β′2
LHON02
LHON01
PAM-R58E02
LHON-AD1b2-3
B
MBON-γ5β′2a
MBON-γ4γ5
SEZON01
SEZON02
SEZON03
LHON01
LHON02
LHON-AD1b2
OTHERS15
OTHERS16
GAL4 lines
0.2
0.0
Proportion of postsynaptic budget
C
MBONs
α2sc
γ1pedc>α/β
Calyx
α′3m
α′3a
α2p3p
α′2
α1
α3
α′3ap
β′2mp
γ4γ5
γ3β′1
γ2γ4/γ2
γ3
γ2
γ1γ2γ3γ4
β′2mp bilateral
β2β′2a
β1>α
γ1γ2
γ4>γ1γ2
γ2α′1
γ5β′1
0.1
0.0
Proportion of postsynaptic budget
D
1.0
0.0
Proportion of DAN inputs downstream of MBONs
E Sugar reward memory
Training
Test
32°C
23°C
min -30
0
30
Performance Index
0.6
0.4
0.2
0.0
-0.2
wildtype>Shits1
PAM (R58E02)>Shits1
SEZON01>Shits1
SEZON02>Shits1
SEZON03>Shits1
F Bitter taste memory
Training Test
32°C
23°C
-30
0
7.5
Performance Index
0.4
0.2
0.0
0.2
-0.4
wildtype>Shits1
PAM (R58E02)>Shits1
SEZON01>Shits1
SEZON02>Shits1
SEZON03>Shits1
G Connectivity to PPL1-γ1pedc dendritic compartments
SIP
SMP
CREd
CREv
SEZON01
OTHER16
SEZON02
OTHER15
MBON-γ4γ5
33
7
2
3
2
47
120
6
24
130
0
number of inputs

Figure 3

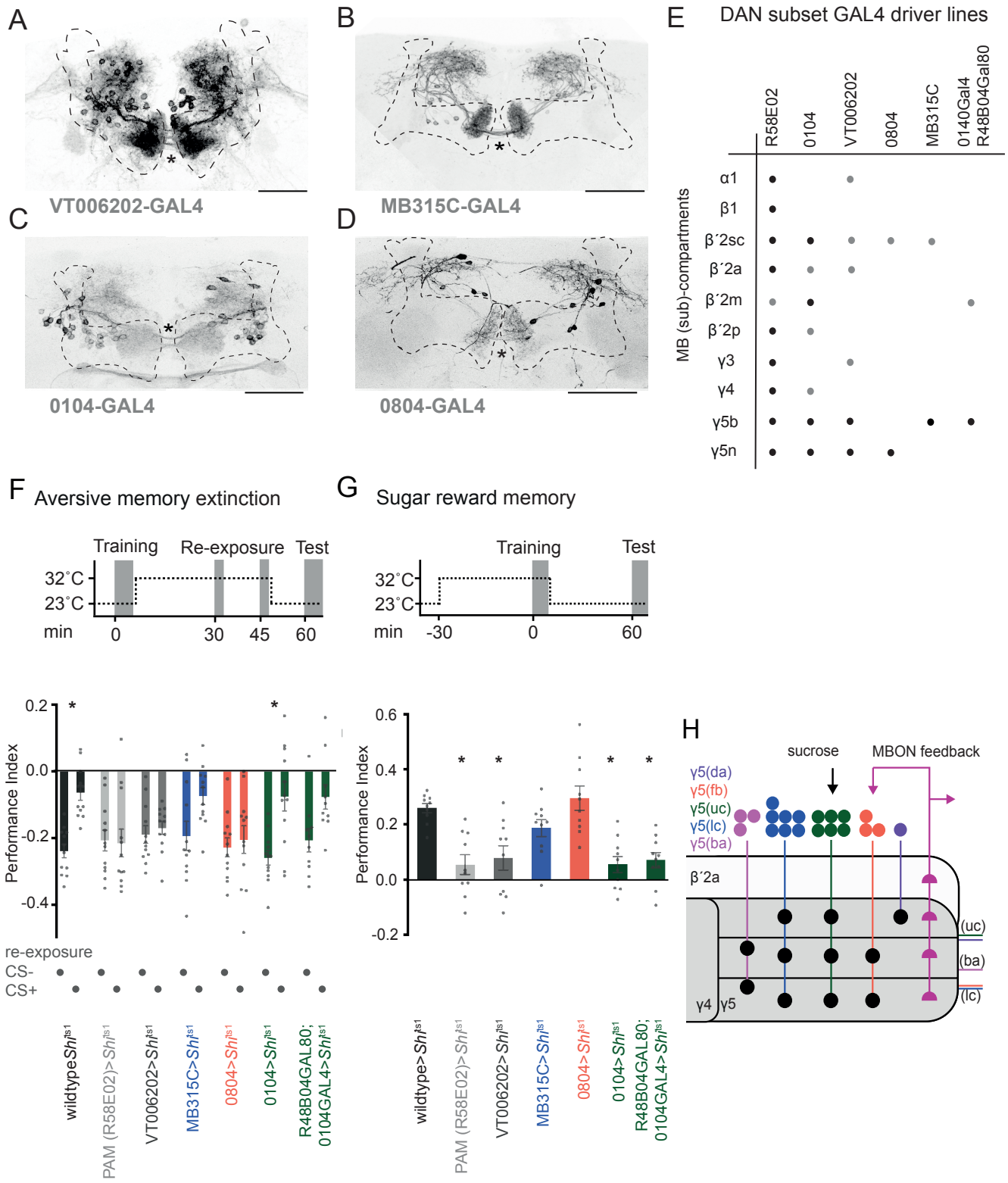
A
VT006202-GAL4
B
MB315C-GAL4
C
0104-GAL4
D
0804-GAL4
E
DAN subset GAL4 driver lines
R58E02
0104
VT006202
0804
MB315C
0140Gal4
R48B04Gal80
MB (sub)-compartments
α1
β1
β´2sc
β´2a
β´2m
β´2p
γ3
γ4
γ5b
γ5n
F
Aversive memory extinction
Training
Re-exposure
Test
32˚C
23˚C
min
0
30
45
60
G
Sugar reward memory
Training
Test
32˚C
23˚C
min
-30
0
60
Performance Index
0.2
0.0
-0.2
-0.4
re-exposure
CS-
CS+
wildtypeShits1
PAM (R58E02)>Shits1
VT006202>Shits1
MB315C>Shits1
0804>Shits1
0104>Shits1
R48B04GAL80; 0104GAL4>Shits1
Performance Index
0.6
0.4
0.2
0.0
-0.2
wildtype>Shits1
PAM (R58E02)>Shits1
VT006202>Shits1
MB315C>Shits1
0804>Shits1
0104>Shits1
R48B04GAL80; 0104GAL4>Shits1
H
sucrose
MBON feedback
γ5(da)
γ5(fb)
γ5(uc)
γ5(lc)
γ5(ba)
β´2a
(uc)
(ba)
(lc)
γ4
γ5

Figure 4